



Deposited via The University of Leeds.

White Rose Research Online URL for this paper:

<https://eprints.whiterose.ac.uk/id/eprint/238220/>

Version: Accepted Version

---

**Article:**

Hughes, D.W., Proctor, M.R.E. and Eltayeb, I.A. (Accepted: 2026) Maxwell-Cattaneo double-diffusive convection: the general case. *Journal of Fluid Mechanics*. ISSN: 0022-1120 (In Press)

---

This is an author produced version of an article accepted for publication in *Journal of Fluid Mechanics*, made available via the University of Leeds Research Outputs Policy under the terms of the Creative Commons Attribution License (CC-BY), which permits unrestricted use, distribution and reproduction in any medium, provided the original work is properly cited.

**Reuse**

This article is distributed under the terms of the Creative Commons Attribution (CC BY) licence. This licence allows you to distribute, remix, tweak, and build upon the work, even commercially, as long as you credit the authors for the original work. More information and the full terms of the licence here:

<https://creativecommons.org/licenses/>

**Takedown**

If you consider content in White Rose Research Online to be in breach of UK law, please notify us by emailing [eprints@whiterose.ac.uk](mailto:eprints@whiterose.ac.uk) including the URL of the record and the reason for the withdrawal request.

Banner appropriate to article type will appear here in typeset article

# 1 **Maxwell-Cattaneo double-diffusive convection: the** 2 **general case**

3 **D.W. Hughes<sup>1†</sup>, M.R.E. Proctor<sup>2</sup> and I.A. Eltayeb<sup>3</sup>**

4 <sup>1</sup>School of Mathematics, University of Leeds, Leeds LS2 9JT, UK

5 <sup>2</sup>DAMTP, Centre for Mathematical Sciences, Wilberforce Road, Cambridge CB3 0WA, UK

6 <sup>3</sup>The Faculty of Mathematical Sciences and Informatics, University of Khartoum, POB 321, Khartoum,  
7 Sudan

8 (Received xx; revised xx; accepted xx)

9 Double-diffusive convection, in which the density of a fluid is dependent on two fields  
10 that diffuse at different rates (such as temperature and salinity), has been widely studied in  
11 areas as diverse as the oceans and stellar atmospheres. Under the assumption of classical  
12 Fickian diffusion for both heat and salt, the evolution of temperature and salinity is governed  
13 by parabolic advection-diffusion equations. In reality, there are small additional terms in  
14 these equations that render them hyperbolic (the Maxwell-Cattaneo effect). Although these  
15 corrections are nominally small, they represent a singular perturbation and hence can lead to  
16 significant effects when the underlying differences of salinity and temperature are large. In  
17 an earlier paper (Hughes, Proctor & Eltayeb 2021 *J. Fluid Mech.* **927**, A13), we investigated  
18 the linear stability of a double-diffusive fluid layer subject to the Maxwell-Cattaneo effect  
19 in either the temperature or the salinity equation (but not both). Here we consider the  
20 general, and much more complicated, case in which the Maxwell-Cattaneo effect influences  
21 both temperature and salinity. We find that, as in the earlier paper, oscillatory instability  
22 is indeed facilitated (and in fact made possible when the salinity gradient is destabilising,  
23 where the classical problem has no oscillatory instability) when the salinity gradients are  
24 sufficiently large. The scalings that emerge from the earlier paper, however, are not necessarily  
25 representative of those in the general case, thus justifying the present study. In addition, we  
26 have found a remarkable singular situation when the ratio of the Maxwell-Cattaneo effects  
27 is equal to the ratio between the heat and salinity diffusivities, near which instability is  
28 strongly enhanced and the critical wavenumber sharply reduced. In addition to determining  
29 the stability boundaries we have also investigated the growth rates of unstable modes and  
30 shown that these are on a par with those of classical double-diffusive convection.

31 **Key words:** double-diffusive convection, general fluid mechanics.

---

† Email address for correspondence: d.w.hughes@leeds.ac.uk



## 1. Introduction

Double-diffusive convection, driven by density variations that are dependent on two fields that diffuse at different rates, is an important process in many geophysical and astrophysical contexts. The most widely studied such problem, applicable to ocean dynamics, is that of thermohaline convection, in which the rapidly diffusing component is heat and the slowly diffusing component salinity (e.g. Huppert & Turner 1981; Radko 2013). Double-diffusive convection in which the competing elements are the variations in composition and temperature can play a role in the planetary context of crystallisation in magmas (Huppert & Sparks 1984) and in the astrophysical context of mixing in the dynamics of deep stellar interiors (e.g. Kato 1966; Merryfield 1995; Garaud 2018). Interchange instabilities driven by magnetic buoyancy, in which the density depends on variations in magnetic pressure and entropy, and which are believed to be important for the release of magnetic flux from stellar interiors, can also, after a transformation of the governing variables, be understood in terms of the classical double-diffusive problem (see Hughes & Proctor 1988; Hughes & Brummell 2021).

Problems in double-diffusive convection have been extensively investigated over the last half-century, with the common feature that the buoyancy-affecting fields diffuse according to the classic Fickian law (for heat transport, also known as the Fourier law), in which the flux of heat or salt is directly proportional to the temperature or salinity gradient. The temperature  $T$ , for example, then obeys the diffusion-advection equation  $D T / D t = \nabla \cdot ((K / \rho c_p) \nabla T)$ , where  $D / D t$  is the usual Lagrangian derivative,  $K$  is the thermal conductivity,  $\rho$  is the density and  $c_p$  is the specific heat at constant pressure. This parabolic equation is necessarily an approximation: it violates relativity, for example, in that information is propagated at infinite speed; nor does it properly account for the detailed nature of heat transport in materials. Maxwell (1867) proposed an improved formulation that replaced the instantaneous nature of the Fickian flux-gradient relation by a modified form in which the flux adjusts in a finite relaxation time  $\tau_T$ ; the usual Fickian law is recovered by setting  $\tau_T = 0$ . The accuracy of the Fourier Law for experiments involving simple classical fluids suggests that  $\tau_T$  is usually very small, as shown in Carrassi & Morro (1972), where it is suggested that  $\tau_T$  can be as small as  $10^{-9}$ s for gases. However, for more complex fluids,  $\tau_T$  can be much larger. For example, Neuhauser (1987), in her investigation of thermal relaxation in superfluid helium-3, found that  $\tau_T$  has values in the range 30 – 400s; Mohammadein (2006), in his study of the thermal relaxation time in two-phase bubbly flow, found that the relaxation time varied between  $10^{-3}$ s and 3s. The reader is referred to Paper I for a fuller discussion of the many related earlier papers that include the M-C effect for temperature.

Maxwell's formulation (now known as the Maxwell-Cattaneo or M-C effect), refined by Christov (2009), leads to unchanged stability criteria for direct (steady) bifurcations from a stationary state with vertical buoyancy gradients, but permits new oscillatory instabilities in certain cases. While the correction term is very small in many instances, it can become important when the density gradients due to heat and salinity are very large. A first attempt at understanding the role of the M-C effect in determining the threshold for double-diffusive instability was made by Hughes *et al.* (2021) — hereinafter referred to as Paper I. They investigated the effect on the linear stability boundary in the two special cases where the M-C formulation was applied either to the temperature field alone, or the salinity field alone. The importance of the new effect is measured (in the case of temperature) by the dimensionless quantity  $C_T = \tau_T K / (2 \rho c_p d^2) = \tau_T \kappa / 2 d^2$  where  $d$  is a typical length scale, and  $\kappa$  is the thermal diffusivity ( $\rho$  and  $K$  are now assumed constant). Analogous remarks apply to the salinity field, leading to the equivalent coefficient  $C_S = \tau_S \kappa_S / 2 d^2$ , where  $\tau_S$  is the relaxation time for the salinity and  $\kappa_S$  is the salt diffusivity. Experimental estimates for

81  $\tau_S$  remain elusive. We shall be concerned with simple Newtonian fluids, for which  $C_T$  and  
82  $C_S$  will be very small.

83 In Paper I it is shown that, even when  $C_S$  or  $C_T$  is very small, M-C effects can become  
84 significant provided that the salt Rayleigh number  $Rs$ , measuring the buoyancy gradient due  
85 to salinity, is large, in that  $RsC^n = O(1)$ , where  $n \geq 1$  and  $C$  denotes either  $C_T$  or  $C_S$ .  
86 In Paper I, the two limiting cases, in which either  $C_S$  or  $C_T$  vanish, were investigated in  
87 detail. It is shown there that when  $n \geq 2$ , the threshold for oscillatory instability is markedly  
88 changed from the classical problem, with oscillations at small horizontal scales becoming the  
89 favoured mode of convection. Indeed, in the case that the salinity gradient is destabilising and  
90 the temperature gradient stabilising (i.e. the fingering regime), oscillations can be preferred  
91 even though they are not possible in the classical case.

92 The question then arises as to the situation when  $C_S$  and  $C_T$  are both non-zero. It is  
93 important to understand whether the scaling laws revealed in Paper I are typical of this more  
94 general case, and also to discover whether new phenomena can occur for particular values  
95 of the ratio  $C_T/C_S$ , with  $C_T$  and  $C_S$  both being small. Thus we revisit the stability problem  
96 in the more general case in which  $C_S$  and  $C_T$  are both non-zero but small, and investigate  
97 the effect of changing the ratio between them. As in Paper I, we consider the distinguished  
98 limit with  $C \ll 1$ ,  $Rs \sim C^{-n}$ ; it is important to note that such a distinguished limit is very  
99 different from the case of  $C \rightarrow 0$  with all other parameters fixed.

100 The analysis in the general case turns out to be more challenging than in Paper I: the  
101 dispersion relation for the growth rate is now fifth order, and untangling the wavenumber  
102 dependence of the preferred modes of instability is more involved. Nonetheless, analytical  
103 progress can be made in general when  $n$  is sufficiently large. We find a variety of behaviours  
104 as the ratio  $C_S/C_T$  is varied. In some cases, the end-point analysis of Paper I gives a good  
105 guide to the behaviour in the more general case. However, we have also identified novel results  
106 completely unrelated to those of Paper I; of particular note is the anomalous behaviour of  
107 the critical values of  $Ra$  and the wavenumber when  $C_S/\kappa_S = C_T/\kappa$  (i.e.  $\tau_T = \tau_S$ ).

108 The layout of the paper is as follows. In § 2 we set out the governing equations and derive  
109 the fifth-order dispersion relation that determines the stability boundary. Sections 3 and 4  
110 investigate respectively the nature of this boundary in the first quadrant of the  $(Rs, Ra)$  plane  
111  $(Rs, Ra > 0)$  and the third quadrant  $(Rs, Ra < 0)$ . Within both § 3 and § 4, behaviour for  
112  $n \lesssim 2$  is considered before the more extreme (and more analytically tractable) situation where  
113  $n \gtrsim 3$ . The anomalous region where  $C_S/\kappa_S \approx C_T/\kappa$  in the first quadrant is treated in detail in  
114 § 3; in the third quadrant we find that steady convection is preferred in this region, as shown  
115 in § 4. In § 5 we investigate the growth rates of unstable modes beyond the stability boundary.  
116 We conclude in § 6 with a discussion of the results and prospects for future work.

## 117 2. Mathematical formulation

### 118 2.1. Maxwell-Cattaneo diffusion

119 To derive the governing equations, it is necessary to consider the modifications from the  
120 M-C effect to be expected in an incompressible fluid moving with velocity  $\mathbf{u}$ . As in Paper I,  
121 in which further details may be found, here we follow the formulation of Christov (2009),  
122 which leads to the equation

$$123 \tau_T \left[ \frac{\partial Q_T}{\partial t} + \nabla \cdot (\mathbf{u} Q_T) \right] = -Q_T - K \nabla^2 T, \quad (2.1)$$

124 where  $Q_T$  is the divergence of the heat flux and where we have assumed that  $K$  is constant.  
125 As  $\mathbf{u}$  is incompressible, the left hand side of (2.1) can be written as the usual Lagrangian

126 derivative of  $Q_T$ . The equation for the salt flux may be obtained, analogously, as

$$127 \quad \tau_S \left[ \frac{\partial Q_S}{\partial t} + \nabla \cdot (\mathbf{u} Q_S) \right] = -Q_S - \kappa_S \nabla^2 S. \quad (2.2)$$

128 We note that the relation between salt flux and salt concentration differs from that between  
129 heat flux and temperature; hence the appearance of  $K$  in (2.1) but  $\kappa_S$  in (2.2).

## 130 2.2. Governing equations

131 As in Paper I, we consider a horizontal layer of an incompressible (Boussinesq) viscous  
132 Maxwell-Cattaneo fluid, initially at rest, contained between two planes at  $z = 0$  (bottom) and  
133  $z = d\pi$  (top). The fluid has kinematic viscosity  $\nu$ , and thermal and salt diffusivities  $\kappa$ ,  $\kappa_S$ . The  
134 density depends linearly on two components that diffuse at different rates. In equilibrium,  
135 the fluid is at rest, with temperature and salinity differences across the layer of  $\Delta T$  and  $\Delta S$ .  
136 The basic state temperature and salinity,  $\bar{T}$  and  $\bar{S}$ , are thus given by

$$137 \quad \bar{T} = T_0 + \Delta T(1 - z/d\pi), \quad \bar{S} = S_0 + \Delta S(1 - z/d\pi), \quad (2.3)$$

138 where  $T_0$  and  $S_0$  are representative values of temperature and salinity. For the perturbed state,  
139 with velocity  $\mathbf{u} = (u, v, w)$ , we express the temperature and salinity by  $T = \bar{T} + \hat{T}$ ,  $S = \bar{S} + \hat{S}$ .  
140 The density  $\rho$  of the fluid obeys a linear relation of the form

$$141 \quad \rho = \rho_0 (1 - \alpha_T (T - T_0) + \alpha_S (S - S_0)), \quad (2.4)$$

142 where  $\rho_0 = \rho(T_0, S_0)$ , and  $\alpha_T$  and  $\alpha_S$  are (constant) coefficients of expansion. The crucial  
143 difference in the governing equations for the Maxwell-Cattaneo system, in comparison with  
144 those of classical double-diffusive convection (with no M-C effects), is the replacement of  
145 the classical Fick's law equations for  $T$  and  $S$  by the modified equations (2.1) and (2.2). On  
146 adopting the standard scalings for distance, time, velocity, heat flux, temperature, salinity  
147 flux, salinity and pressure of  $d$ ,  $d^2/\kappa$ ,  $\kappa/d$ ,  $\Delta TK/d$ ,  $\Delta T$ ,  $\Delta S\kappa_S/d$ ,  $\Delta S$  and  $\rho_0\nu\kappa/d^2$ , and  
148 dropping the hats, the governing equations take the form

$$149 \quad \frac{1}{\sigma} \frac{D\mathbf{u}}{Dt} = -\nabla p + RaT\hat{z} - RsS\hat{z} + \nabla^2 \mathbf{u}, \quad (2.5)$$

$$150 \quad \nabla \cdot \mathbf{u} = 0, \quad (2.6)$$

$$151 \quad \frac{DT}{Dt} = w - Q_T, \quad (2.7)$$

$$152 \quad 2C_T \frac{DQ_T}{Dt} = -Q_T - \nabla^2 T, \quad (2.8)$$

$$153 \quad \frac{DS}{Dt} = w - Q_S, \quad (2.9)$$

$$154 \quad 2C_S \frac{DQ_S}{Dt} = -Q_S - \tau \nabla^2 S, \quad (2.10)$$

156 where the Rayleigh number  $Ra$ , the salt Rayleigh number  $R_S$ , the Prandtl number  $\sigma$ , and the  
157 diffusivity ratio  $\tau$  are defined by

$$158 \quad Ra = \frac{g\alpha_T \Delta T d^3}{\kappa\nu}, \quad R_S = \frac{g\alpha_S \Delta S d^3}{\kappa\nu}, \quad \sigma = \frac{\nu}{\kappa}, \quad \tau = \frac{\kappa_S}{\kappa}. \quad (2.11)$$

159 With the Rayleigh numbers so defined, positive (negative)  $Ra$  is thermally destabilising  
160 (stabilising), whereas positive (negative)  $R_S$  is solutally stabilising (destabilising).

161 These governing equations are the same as those derived in Paper I, where we examined

162 the limiting cases of  $C_S = 0$  and  $C_T = 0$ . Our aim here is to understand the nature of any  
 163 instability in between these two limits. Thus, rather than working with  $C_T$  and  $C_S$  directly, it  
 164 is instructive to define two new parameters:

$$165 \quad \Gamma = C_S + C_T, \quad \lambda = \frac{C_S - C_T}{C_S + C_T}. \quad (2.12)$$

166 For certain parts of the analysis, it is also convenient to work with the quantities

$$167 \quad \lambda_1 = \frac{C_S}{\Gamma} = \frac{1}{2}(1 + \lambda), \quad \lambda_2 = \frac{C_T}{\Gamma} = \frac{1}{2}(1 - \lambda), \quad \alpha = \frac{C_S}{C_T} = \frac{\lambda_1}{\lambda_2}. \quad (2.13)$$

168 We shall be interested in the case of  $\Gamma \ll 1$  (i.e.  $C_T$  and  $C_S$  both small);  $\lambda$  varies between  $-1$   
 169 ( $C_S = 0$ ) and  $+1$  ( $C_T = 0$ ).

### 170 *2.3. Linearisation and stability considerations*

171 As in Paper I, we address the linear stability of the basic state given by (2.3) and (2.4), subject  
 172 to the standard boundary conditions in which the horizontal boundaries are impermeable and  
 173 stress-free, and on which the temperature and salinity are fixed. Thus

$$174 \quad \frac{\partial u_x}{\partial z} = \frac{\partial u_y}{\partial z} = u_z = T = S = 0 \quad \text{on } z = 0, \pi, \quad (2.14)$$

175 noting that  $z$  is now dimensionless. We assume periodicity in the horizontal directions. In  
 176 general, we may decompose the solenoidal velocity as

$$177 \quad \mathbf{u} = \nabla \times (\nabla \times \mathcal{P} \hat{\mathbf{z}}) + \nabla \times \mathcal{T} \hat{\mathbf{z}}. \quad (2.15)$$

178 The linearised form of (2.5) shows, however, that  $\mathcal{T}$  decays for all parameter values, and  
 179 thus only  $\mathcal{P}$  is of relevance. Following the usual approach to the classical double-diffusive  
 180 stability problem, we seek solutions to the linearised versions of (2.5) – (2.10) of the form

$$181 \quad \mathcal{P} \propto T \propto S \propto Q_T \propto Q_S \propto f(x, y) \sin m z e^{st}, \quad (2.16)$$

182 where the planform function  $f(x, y)$  satisfies

$$183 \quad \nabla_H^2 f = -k^2 f, \quad (2.17)$$

184 with  $\nabla_H^2$  being the horizontal Laplacian. For the classical problem, with no M-C effects  
 185 (i.e.,  $\Gamma = 0$ ), it is readily shown that the fundamental mode (i.e.  $m = 1$ ) is the most readily  
 186 destabilised. Here we shall also restrict attention to the  $m = 1$  mode, but will discuss this  
 187 assumption in § 6, in the light of the results.

188 On substitution from (2.16) into the linearised forms of (2.5) – (2.11), we obtain, after  
 189 some algebraic manipulation, a quintic dispersion relation for the growth rate  $s$ :

$$190 \quad a_5 s^5 + a_4 s^4 + a_3 s^3 + a_2 s^2 + a_1 s + a_0 = 0, \quad (2.18)$$

191 where

$$192 \quad a_5 = \frac{\Gamma^2(1 - \lambda^2)\beta^2}{\sigma}, \quad (2.19a)$$

$$193 \quad a_4 = \frac{2\Gamma}{\sigma}\beta^2 + \Gamma^2(1 - \lambda^2)\beta^4, \quad (2.19b)$$

$$194 \quad a_3 = \frac{\beta^2}{\sigma} + \frac{\Gamma}{\sigma}(1 + 2\sigma + \tau + \lambda(1 - \tau))\beta^4 + \Gamma^2(1 - \lambda^2)(Rs - Ra)k^2, \quad (2.19c)$$

$$195 \quad a_2 = \left(1 + \frac{1 + \tau}{\sigma}\right)\beta^4 + \Gamma(1 + \tau + \lambda(1 - \tau))\beta^6 + 2\Gamma(Rs - Ra)k^2, \quad (2.19d)$$

$$196 \quad a_1 = \left(1 + \tau + \frac{\tau}{\sigma}\right)\beta^6 + Rs\left(1 + \Gamma(1 + \lambda)\beta^2\right)k^2 - Ra\left(1 + \tau\Gamma(1 - \lambda)\beta^2\right)k^2, \quad (2.19e)$$

$$197 \quad a_0 = \tau\beta^8 + Rs\beta^2k^2 - \tau Ra\beta^2k^2, \quad (2.19f)$$

199 and where  $\beta^2 = k^2 + 1$ . As shown in Paper I, the symmetry of the system allows us to consider  
200 only the case of  $\tau < 1$ .

201 In this paper, we shall concentrate on determining the conditions for the onset of instability;  
202 this may occur either as a direct mode (steady convection), in which case the growth rate  
203  $s$  passes through zero, or as an oscillatory mode, in which case, at onset,  $s = \pm i\omega$ , with  
204  $\omega \in \mathbb{R}_+$ . It is traditional in studies of double-diffusive convection to treat  $Ra$  as the bifurcation  
205 parameter, although, mathematically, there is nothing to favour  $Ra$  over  $Rs$ . For comparison  
206 with the existing literature, we shall maintain this tradition here. We shall denote  $Ra(k^2)$  at  
207 the onset of steady (oscillatory) convection by  $Ra^{(s)}$  ( $Ra^{(o)}$ ), the minimum of  $Ra^{(s)}$  ( $Ra^{(o)}$ )  
208 over all wavenumbers as  $Ra_c^{(s)}$  ( $Ra_c^{(o)}$ ), the associated value of  $k^2$  by  $k_{sc}^2$  ( $k_{oc}^2$ ), and, for the  
209 case of oscillatory onset, the associated value of  $\omega^2$  by  $\omega_c^2$ . The lesser of  $Ra_c^{(s)}$  and  $Ra_c^{(o)}$  is  
210 the overall critical Rayleigh number, which we denote by  $Ra_c$ , with  $k^2 = k_c^2$ . We shall refer  
211 to the mode that first becomes unstable as  $Ra$  is increased as the *preferred* or *favoured* mode.

212 From the form of the flux equations (2.8) and (2.10) it is clear that M-C effects only occur  
213 in time-derivative terms, so these effects have no influence on the onset of steady convection.  
214 The value of  $Ra$  at the onset of steady convection is therefore given by

$$215 \quad Ra = Ra^{(s)} = \frac{Rs}{\tau} + \frac{\beta^6}{k^2}. \quad (2.20)$$

216 Since  $\beta^6/k^2$  is minimised when  $k^2 = 1/2$ ,

$$217 \quad Ra_c^{(s)} = \frac{Rs}{\tau} + \frac{27}{4}. \quad (2.21)$$

218 To determine the onset of oscillatory instability, we set  $s = \pm i\omega$ , with  $\omega \in \mathbb{R}_+$ , leading to  
219 the coupled equations

$$220 \quad a_5\omega^4 - a_3\omega^2 + a_1 = 0, \quad a_4\omega^4 - a_2\omega^2 + a_0 = 0. \quad (2.22a,b)$$

221 Since  $Ra$  and  $Rs$  occur linearly in coefficients  $a_0, a_1, a_2, a_3$  — and are absent in  $a_4$  and  $a_5$   
222 — we can combine equations (2.22) to derive a cubic equation for  $\omega^2$  that does not involve  
223  $Ra$  (or, alternatively,  $Rs$ ), or eliminate  $\omega^2$  to derive an expression cubic in  $Ra$  and  $Rs$ . In  
224 Paper I, the corresponding expressions were quadratic rather than cubic, and we made use  
225 of each. Here the expressions for the coefficients of the cubic in  $Ra$  are extremely lengthy,  
226 and so, with one exception, our primary mode of attack will be via the cubic equation for  $\omega^2$ ,  
227 which takes the form:

$$228 \quad b_6\omega^6 + b_4\omega^4 + b_2\omega^2 + b_0 = 0, \quad (2.23)$$

229 where

$$230 \quad b_6 = \sigma \Gamma^4 (1 - \lambda^2)^2 \beta^2, \quad (2.24a)$$

$$231 \quad b_4 = \Gamma^2 (2\sigma(1 + \lambda^2) + (1 + \lambda)^2) \beta^2 - \sigma \Gamma^3 (1 - \lambda^2) (1 + 2\tau + \lambda(1 - 2\tau)) \beta^4, \quad (2.24b)$$

$$232 \quad b_2 = (1 + \sigma) \beta^2 - \Gamma (\sigma + 2\tau(1 + \sigma) + \lambda (2\tau(1 + \sigma) - \sigma)) \beta^4 \\ 233 \quad + \sigma \Gamma^2 ((\tau - 1) \lambda^2 - 2(1 + \tau) \lambda + \tau - 1) R s k^2 \quad (2.24c)$$

$$234 \quad + \sigma \tau \Gamma^2 ((\tau - 2) \lambda^2 - 2\tau \lambda + 2 + \tau) \beta^6, \quad (2.24d)$$

$$235 \quad b_0 = \tau^2 (1 + \sigma) \beta^6 - \Gamma (1 - \lambda) \sigma \tau^2 \beta^8 - \sigma (1 - \tau) R s k^2 + 2\sigma \tau \Gamma \lambda R s \beta^2 k^2. \quad (2.24e)$$

237 For completeness, the cubic equation determining  $Ra^{(o)}$  is contained in the supplementary  
238 material.

239 We recap briefly the results for the classical double-diffusive problem; more details can be  
240 found in Paper I. Oscillatory instability can occur only in the first quadrant of the  $(Rs, Ra)$   
241 plane (i.e.  $Rs$  and  $Ra$  both positive); this is often referred to as the diffusive regime. The  
242 marginal value of  $Ra$  for oscillatory motions (i.e. when  $s = \pm i\omega$ ,  $\omega \in \mathbb{R}_+$ ) is given by

$$243 \quad Ra^{(o)} = \left( \frac{\sigma + \tau}{1 + \sigma} \right) R s + \frac{(1 + \tau)(\sigma + \tau) \beta^6}{\sigma k^2}, \quad (2.25)$$

244 provided also that  $\omega^2 > 0$ , which translates to the condition

$$245 \quad R s > \frac{\tau^2 (1 + \sigma) \beta^6}{\sigma (1 - \tau) k^2}. \quad (2.26)$$

246 It follows from (2.26) that oscillatory motions are preferred at onset provided that

$$247 \quad R s > \frac{27 \tau^2 (1 + \sigma)}{4 \sigma (1 - \tau)}; \quad (2.27)$$

248 from (2.25), the critical Rayleigh number for oscillatory convection is then given by

$$249 \quad Ra_c^{(o)} = \left( \frac{\sigma + \tau}{1 + \sigma} \right) R s + \frac{27(1 + \tau)(\sigma + \tau)}{4\sigma}. \quad (2.28)$$

250 In the third quadrant (i.e.  $Rs < 0$ ,  $Ra < 0$ ), instability always occurs as steady convection,  
251 with critical Rayleigh number given by (2.21); this is typically referred to as the salt fingering  
252 regime.

253 In Paper I, we studied the role of the (small) M-C effects by considering different regimes  
254 for (large)  $Rs$ ; this was achieved by scaling  $Rs$  with either  $C_T^{-n}$  (for  $C_S = 0$ ) or  $C_S^{-n}$  (for  
255  $C_T = 0$ ) and investigating the nature of the behaviour with increasing  $n$ . In a similar vein, for  
256 the more general problem considered here, it is instructive to consider the regimes defined  
257 by  $Rs = O(\Gamma^{-n})$ . As discussed above, in the classical problem, it is in the first and third  
258 quadrants of the  $(Rs, Ra)$  plane that double-diffusive effects come into play (in the second  
259 quadrant the fluid is top-heavy and hence unstable to overturning, whereas the fourth quadrant  
260 is a region of stability). Thus, with the inclusion of M-C effects, we examine separately the  
261 behaviour in the first and third quadrants in the  $(Rs, Ra)$  plane.

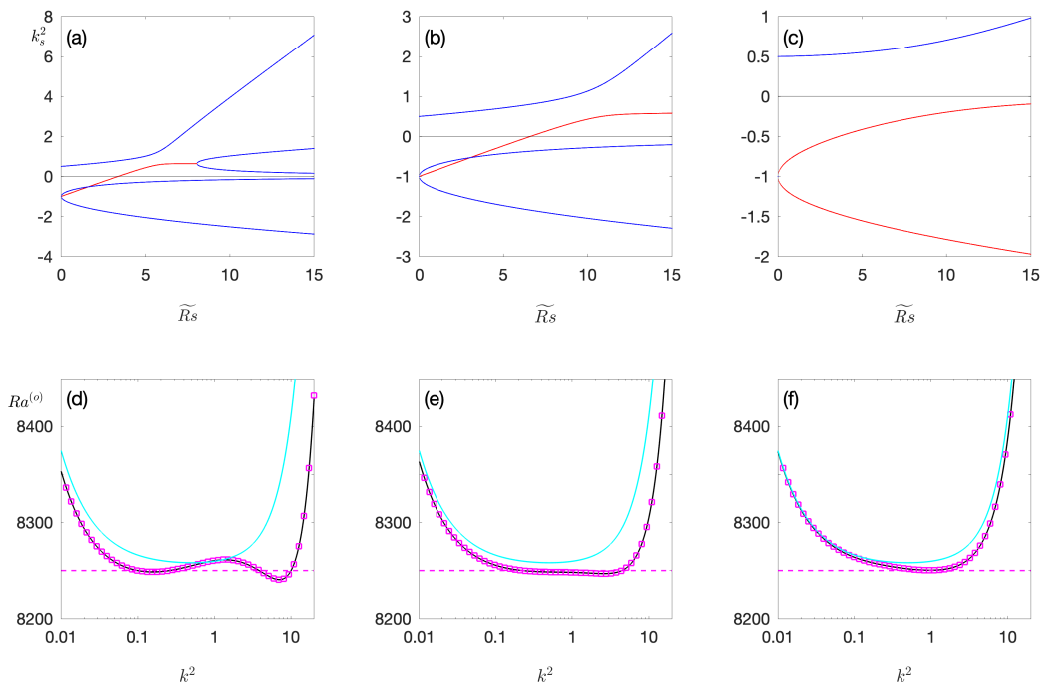


Figure 1: (a-c) The real parts of the roots of (A 6) for  $k_s^2$  as a function of  $\widetilde{R}s$  for  $0 < n \leq 1$ ; blue lines denote real roots, the red line denotes the real part of a conjugate pair;  $\sigma = 1$ ,  $\tau = 0.1$ , with (a)  $\lambda = -0.8$ , (b)  $\lambda = 0$ , (c)  $\lambda = 0.8$ . (d-f) Corresponding plots of the oscillatory stability boundary (grey solid line), together with the zeroth-order asymptotic expression (A 3) (magenta dashed line) and the first-order correction (A 5) (magenta squares); for the numerical results,  $\Gamma = 10^{-3}$ ,  $Rs = 1.5 \times 10^4$  (corresponding to  $\widetilde{R}s = 15$ ). For comparison, the cyan line shows  $Ra^{(o)}$  for the classical problem, given by (2.25).

### 262 3. The first quadrant: $Rs > 0$ , $Ra > 0$

263

#### 3.1. $0 < n \leq 1$

264 When  $Rs$  assumes  $O(1)$  values, the problem is essentially that of classical double-diffusive  
 265 convection. Qualitative changes from the classical problem first arise when  $n = 1$ ; to  
 266 investigate this regime, we rescale both Rayleigh numbers with  $\Gamma^{-1}$ . For classical double  
 267 diffusion, the critical wavenumber for oscillatory convection (and indeed steady convection  
 268 also) is given by  $k^2 = 1/2$ . To explore how the M-C effect can influence this picture, we  
 269 consider the regime  $\Gamma \ll 1$ ,  $Rs = \Gamma^{-1}\widetilde{R}s$ ,  $Ra = \Gamma^{-1}\widetilde{R}a$ , where  $\widetilde{R}s$  and  $\widetilde{R}a$  are  $O(1)$ , and with  
 270  $k = O(1)$ . The details of the associated analysis, which is in the same spirit as for the end  
 271 points  $\lambda = \pm 1$ , though algebraically more messy, are contained in Appendix A. The leading  
 272 order expression for the onset of oscillatory convection ( $\widetilde{R}a_0$ ) is given by (A 3), namely

$$273 \quad \widetilde{R}a_0 = \frac{(\sigma + \tau)}{(1 + \sigma)} \widetilde{R}s \quad \text{or} \quad Ra_0 = \frac{(\sigma + \tau)}{(1 + \sigma)} Rs. \quad (3.1)$$

274 We note that  $\widetilde{R}a_0$  is independent of both  $\lambda$  and  $k$ . Determination of the critical wavenumber  
 275 comes at the next order (i.e. determining  $\widetilde{R}a_1$ ), where  $d\widetilde{R}a_1/dk^2 = 0$  gives rise to a quintic  
 276 polynomial in  $k^2$  (expression (A 6), with coefficients (A 5)). Figures 1(a-c) show the evolution

277 of the real parts of the roots of the quintic polynomial (A 6) as  $\widetilde{R}s$  is increased, for three  
 278 values of  $\lambda$ . With  $Rs = 0$ , the only real positive root is at  $k = 1/2$  (the classical case). For  
 279 all values of  $\lambda$ , the existing mode moves to higher  $k$ . As for  $C_s = 0$  (i.e.  $\lambda = -1$ ), for  $\lambda$   
 280 close to  $-1$ , two equal stationary points appear at a critical value of  $Rs$  ( $Rs^*$ , say) which  
 281 then separate with a further increase in  $Rs$ ;  $k^2$  remains negative (and thus unphysical) for the  
 282 other two roots (see figure 1(a)). As  $\lambda$  increases,  $Rs^*$  increases (it has moved off to the right  
 283 in figure 1(b)), with  $Rs^* \rightarrow \infty$  as  $\lambda \rightarrow \lambda^*$ , where

$$284 \quad \lambda^* = \frac{\sqrt{\sigma + \tau} - \sqrt{\tau(1 + \sigma)}}{\sqrt{\sigma + \tau} + \sqrt{\tau(1 + \sigma)}}. \quad (3.2)$$

285 For  $\lambda > \lambda^*$ , there is only one real stationary point (as in figure 1c). Thus, for  $-1 \leq \lambda < \lambda^*$ ,  
 286 the M–C influence is felt for  $Rs = O(\Gamma^{-1})$  by the emergence of two new stationary points  
 287 in the oscillatory stability boundary. More generally, it can be seen that for all  $\lambda$ , there  
 288 is a shift of the classical mode to higher wavenumbers. Figures 1(d–f) show the oscillatory  
 289 stability boundary with no approximations (calculated numerically), together with the zeroth-  
 290 order approximation  $\widetilde{Ra}_0$ , and with the first-order correction  $\widetilde{Ra}_1$ ; the latter is essentially  
 291 indistinguishable from the boundary of the full system. The oscillatory stability boundary for  
 292 the classical problem, given by (2.25), is also shown. The three stationary points in figure 1(d)  
 293 correspond to the three positive roots for  $k^2$  at  $\widetilde{R}s = 15$  in figure 1(a). Whenever there is more  
 294 than one minimum in the  $Ra^{(o)}$  versus  $k^2$  curve (as in figure 1(d)), the higher wavenumber  
 295 mode is always preferred. We note also that since  $Ra_c^{(s)} \approx Rs/\tau > Ra_0$  (from (2.21)), the  
 296 preferred mode is always oscillatory.

### 297 3.2. $n = 2$

298 It is helpful to begin by summarising the main findings from Paper I of the  $n = 2$  regime for  
 299  $\lambda = \pm 1$ . When  $\lambda = -1$  ( $C_s = 0$ ),  $Ra$ , as a function of  $k^2$ , has two minima: a large wavelength  
 300 mode with  $k^2 = O(C_T)$  and a small wavelength mode with  $k^2 = O(C_T^{-1})$ . The  $k^2 = O(C_T^{-1})$   
 301 mode is always preferred; the onset of instability is oscillatory, with  $Ra_c = O(C_T^{-2})$ . When  
 302  $\lambda = 1$  ( $C_T = 0$ ), there is only one minimum of  $Ra$  as a function of wavenumber, with  
 303  $k^2 = O(C_s^{-1/2})$ ; the onset of instability is oscillatory, with  $Ra_c = O(C_s^{-2})$ . Even for the  
 304 limiting cases of  $\lambda = \pm 1$ , analytical progress in the  $n = 2$  regime was limited, since the only  
 305 simplification is that (at high wavenumbers)  $\beta^2 \approx k^2$ . For  $-1 < \lambda < 1$ , where the behaviour  
 306 is more complex, the  $n = 2$  regime is essentially accessible only to numerical study.

307 Figure 2 shows  $Ra^{(o)}$  as a function of  $k^2$  for a large and small value of  $\sigma$  ( $\sigma = 10$  in (a–c)  
 308 and  $\sigma = 0.1$  in (d–f)), with  $\tau = 0.5$ , and for  $\lambda = -0.8, 0, 0.8$ ; for comparison, the limiting  
 309 values of  $\lambda = -1$  and  $\lambda = 1$  are also shown, respectively, on the  $\lambda = -0.8$  and  $\lambda = 0.8$   
 310 plots. Note that since  $Ra_c^{(s)} \approx Rs/\tau = 2 \times 10^6$ , the oscillatory mode is preferred, and hence  
 311 determines the overall stability boundary. For both values of  $\sigma$ , the qualitative behaviour  
 312 as  $\lambda$  changes is the same. For  $\lambda = -0.8$ , there are two minima in  $Ra^{(o)}$ , as for  $\lambda = -1$ ;  
 313 the preferred mode is at the larger wavenumber, with  $k^2 = O(C_T^{-1})$ . As  $\lambda$  increases, the  
 314 (non-preferred) minimum at small  $k^2$  disappears and the preferred mode moves gradually to  
 315 smaller  $k^2$ . The minima of the  $\lambda = 0.8$  curves are located at slightly larger values of  $k^2$  than  
 316 those at  $\lambda = 1$ , where the preferred mode has  $k^2 = O(C_s^{-1/2})$ . For comparison,  $Ra^{(o)}$  for the  
 317 classical problem, given by (2.25), is also shown in figure 2; for the cases illustrated, it can  
 318 be seen that the M–C effect is a destabilising influence.

319 Figure 3 shows  $Ra_c^{(o)}$ ,  $k_c^2$  and  $\omega_c^2$  as a function of  $\lambda$  for four pairs of  $(\sigma, \tau)$  values. Again,  
 320  $Ra_c^{(s)} \approx Rs/\tau$  exceeds  $Ra_c^{(o)}$ , and so the oscillatory stability boundary determines the overall  
 321 boundary. As shown in Paper I, at both end points ( $\lambda = \pm 1$ ),  $Ra_c^{(o)} = O(\Gamma^{-2})$ , though which

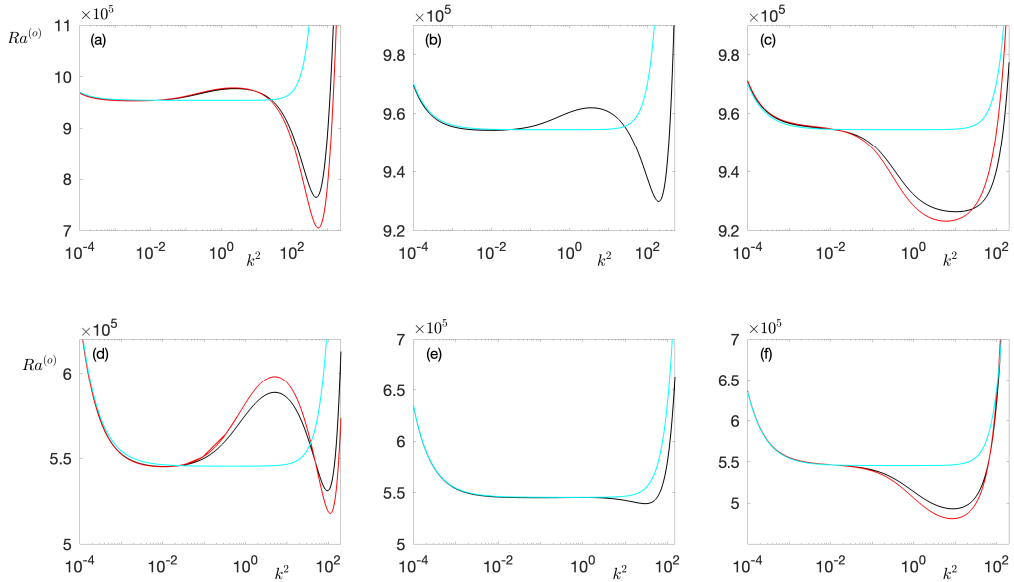


Figure 2:  $Ra^{(o)}$  versus  $k^2$  for  $\Gamma = 10^{-3}$ ,  $Rs = 10^6$  ( $n = 2$ ),  $\tau = 0.5$ . In (a-c),  $\sigma = 10$ , with (a)  $\lambda = -0.8$  (black),  $\lambda = -1$  (red); (b)  $\lambda = 0$ , (c)  $\lambda = 0.8$  (black),  $\lambda = 1$  (red). In (d-f),  $\sigma = 0.1$ , with (d)  $\lambda = -0.8$  (black),  $\lambda = -1$  (red); (e)  $\lambda = 0$ , (f)  $\lambda = 0.8$  (black),  $\lambda = 1$  (red). The cyan lines show  $Ra^{(o)}$  for the classical problem, given by (2.25).

322 of these is the more unstable depends on the values of  $\sigma$  and  $\tau$  (contrast, for example,  
 323 figures 3(a) and (d)). In the displayed numerical results, the most stable configuration has a  
 324 mid-range value of  $\lambda$ . However, at very large  $\sigma$  (not shown) and small values of  $\tau$ ,  $Ra_c^{(o)}$   
 325 essentially increases monotonically with  $\lambda$  over the entire interval; furthermore, for very  
 326 large  $\sigma$  and  $\tau$  close to unity,  $Ra_c^{(o)}$  increases for  $-1 < \lambda \lesssim 0$ , and then exhibits very little  
 327 change over the range  $0 \lesssim \lambda < 1$ . As already noted, the values of  $k_c^2$  at the end points are  
 328 asymptotically distinct. Thus there is inevitably a decrease in  $k_c^2$  from  $\lambda = -1$  to  $+1$ ; this may  
 329 or may not be monotonic, depending on the values of  $\sigma$  and  $\tau$ . Conversely, the frequencies  
 330 at  $\lambda = \pm 1$  both scale as  $\omega_c^2 = O(\Gamma^{-2})$ , a scaling that is maintained throughout the range of  $\lambda$ .  
 331 Figure 3 also shows  $Ra_c^{(o)}$  for the classical problem, given by (2.28). It can be seen that for  
 332 the cases illustrated, the M-C effect, save possibly for a small interval of  $\lambda$ , is destabilising.

333

### 3.3. $n \geq 3$

334 Figure 4 shows  $Ra_c^{(o)}$ ,  $k_c^2$  and  $\omega_c^2$  as functions of  $\lambda$  for  $n = 3, 4, 5$ . The most striking  
 335 feature of the  $n \geq 3$  regime is the appearance of a narrow region close to  $\lambda_1/\lambda_2 = \tau$   
 336 (or  $\lambda = \lambda_d = (\tau - 1)/(\tau + 1)$ ) in which both the critical wavenumber and its associated  
 337 frequency are markedly smaller than at nearby values of  $\lambda$ . This region corresponds to  
 338  $\tau_T = \tau_S$ , as discussed in § 1, and we refer to it as ‘the dip’. The sharp minima in  $k_c^2$  and  $\omega_c^2$   
 339 are accompanied by a sharp maximum in  $Ra_c^{(o)}$ . The analysis below shows that the width  
 340 of the narrow region is  $O(\Gamma^{(n-2)/2})$ , as can be seen in figure 5, which shows a small range  
 341 of  $\lambda$  near  $\lambda_d$ . Figure 6 shows  $Ra_c^{(o)}$  as a function of  $k^2$  for values of  $\lambda$  just to the left of  
 342 the dip, in the dip itself, and just to the right of the dip. The transition of  $k_c^2$  and  $\omega_c^2$  in the  
 343 dip is discontinuous: as  $\lambda$  increases through  $\lambda_d$ , the minimum at larger  $k^2$  (figure 6(a), with

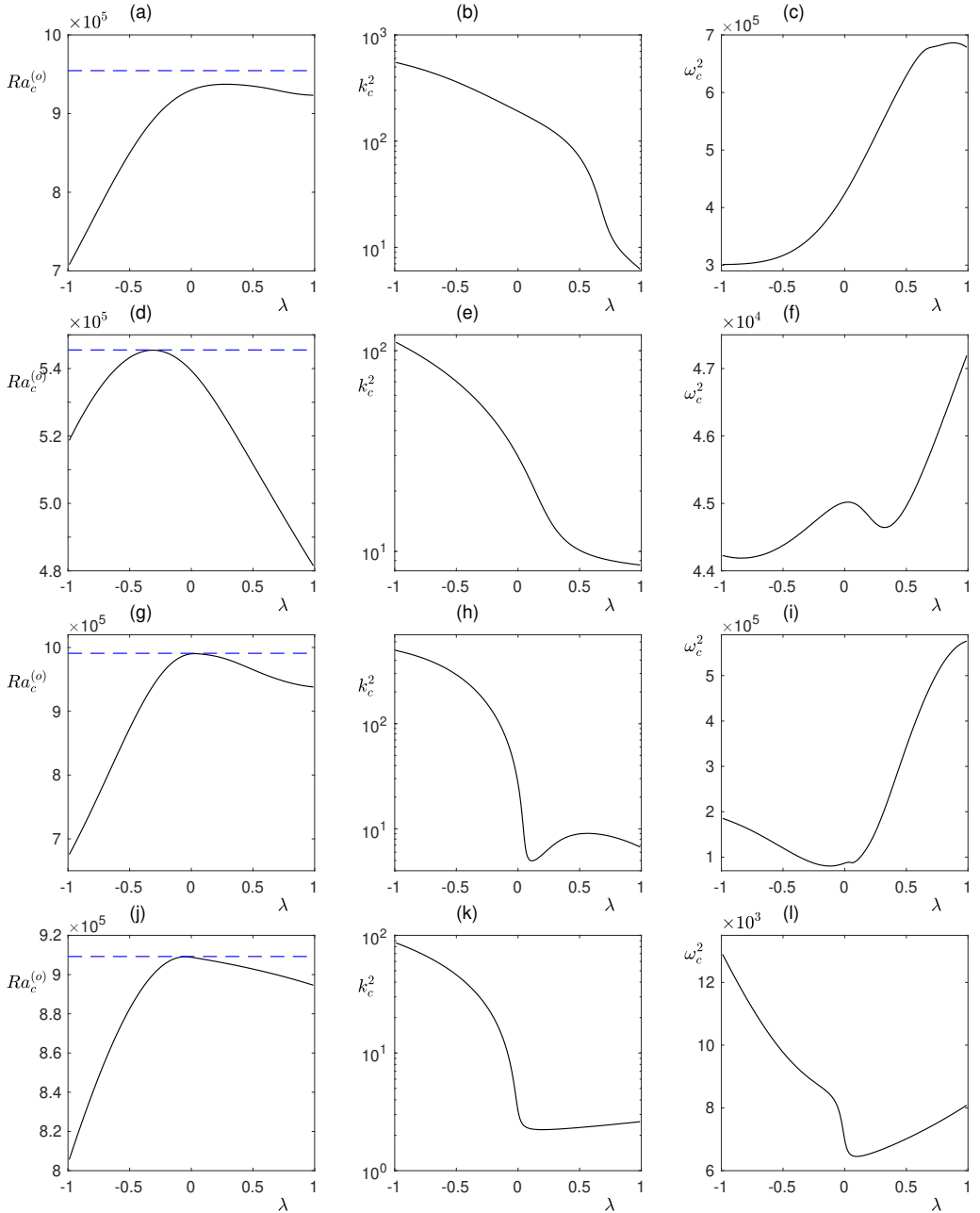


Figure 3:  $Ra_c^{(o)}$ ,  $k_c^2$  and  $\omega_c^2$  versus  $\lambda$  for  $\Gamma = 10^{-3}$ ,  $Rs = 10^6$  ( $n = 2$ ). In (a-c),  $\sigma = 10$ ,  $\tau = 0.5$ ; in (d-f),  $\sigma = 0.1$ ,  $\tau = 0.5$ ; in (g-i),  $\sigma = 10$ ,  $\tau = 0.9$ ; in (j-l),  $\sigma = 0.1$ ,  $\tau = 0.9$ . The blue dashed line shows  $Ra_c^{(o)}$  for the classical problem, given by (2.28).

344  $k_c^2 = 1.77 \times 10^8$ ) becomes higher than that at smaller  $k^2$ , leading to a discontinuous change  
 345 in the critical wavenumber (figure 6(b), with  $k_c^2 = 1.22 \times 10^6$ ), before the minimum at large  
 346  $k^2$  reasserts itself (figure 6(c), with  $k_c^2 = 2.22 \times 10^8$ ).

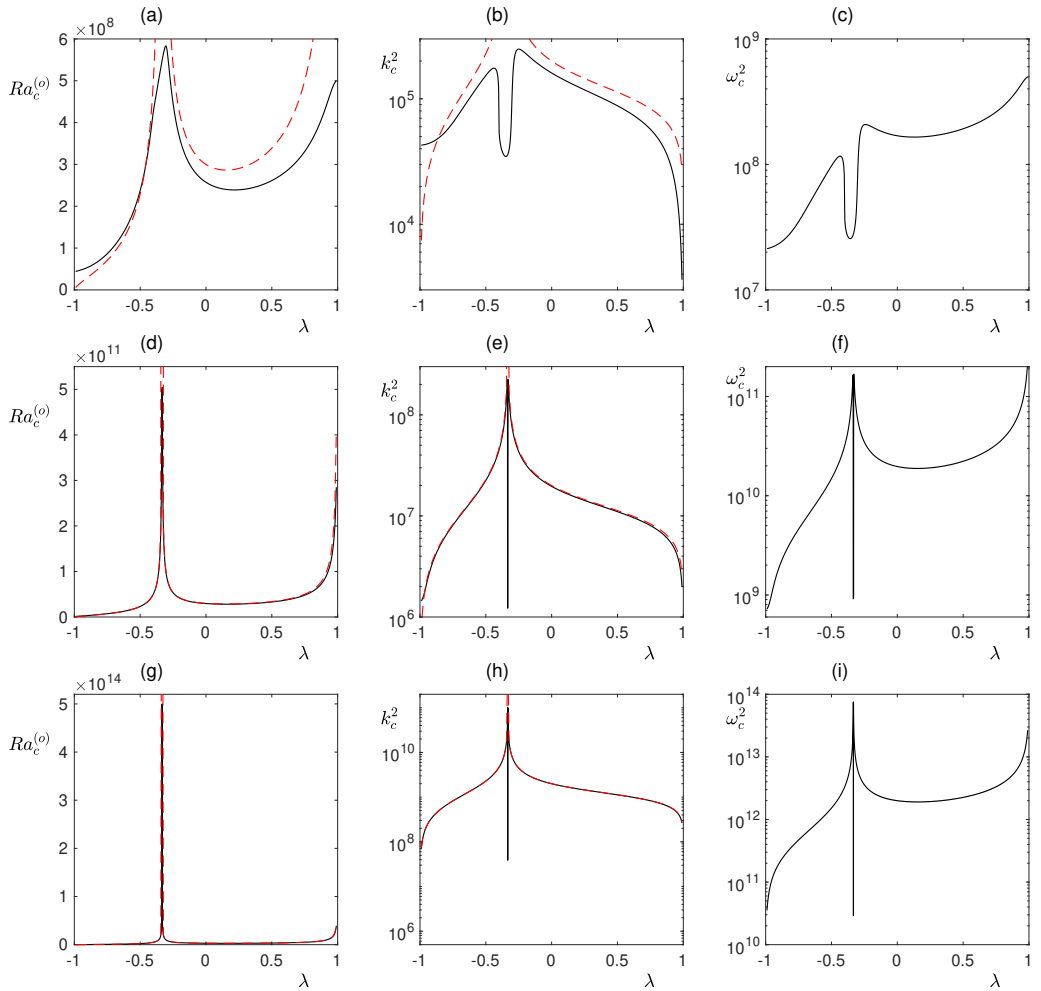


Figure 4:  $Ra_c^{(o)}$ ,  $k_c^2$  and  $\omega_c^2$  versus  $\lambda$  for  $\Gamma = 10^{-3}$ ,  $\sigma = 1$ ,  $\tau = 0.5$ . In (a-c),  $Rs = 10^9$  ( $n = 3$ ); in (d-f),  $Rs = 10^{12}$  ( $n = 4$ ); in (g-i),  $Rs = 10^{15}$  ( $n = 5$ ). The asymptotic results (3.11) are marked as dashed red lines.

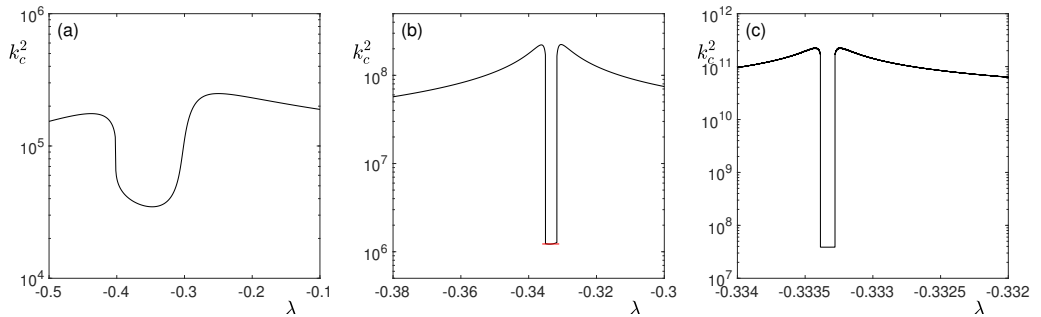


Figure 5:  $k_c^2$  versus  $\lambda$ , for a restricted range of  $\lambda$ , with  $\Gamma = 10^{-3}$ ,  $\sigma = 1$ ,  $\tau = 0.5$ . In (a),  $Rs = 10^9$  ( $n = 3$ ); in (b),  $Rs = 10^{12}$  ( $n = 4$ ); in (c),  $Rs = 10^{15}$  ( $n = 5$ ). In (b), the asymptotic result (3.25) is marked as a red line.

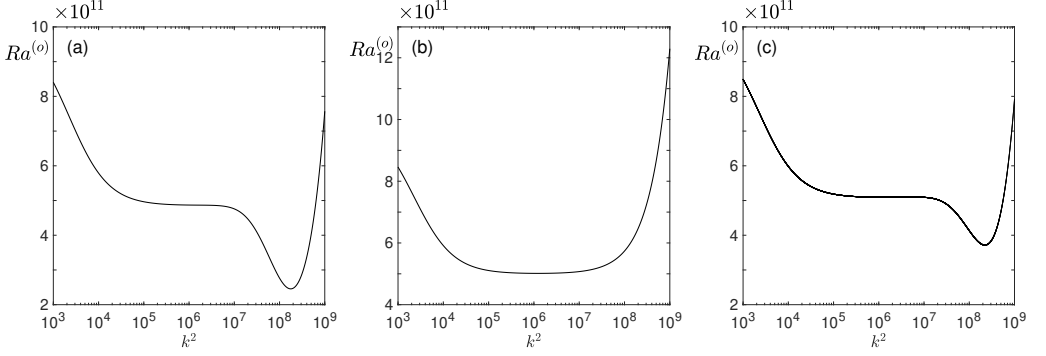


Figure 6:  $Ra^{(o)}$  versus  $k^2$  with  $\Gamma = 10^{-3}$ ,  $Rs = 10^{12}$  ( $n = 4$ ),  $\sigma = 1$ ,  $\tau = 0.5$ . In (a),  $\lambda = -0.34$  (just to the left of the dip); in (b),  $\lambda = -0.3335$  (in the middle of the dip); in (c),  $\lambda = -0.33$  (just to the right of the dip).

### 3.3.1. Asymptotics for general $\lambda$

We can give accurate asymptotic descriptions of the behaviour of the marginal curves in the first quadrant when  $\Gamma \ll 1$  and  $n \geq 3$  (the larger the value of  $n$  the more accurate the results). To begin with, we consider the general case away from the dip, so that  $\lambda_1/\lambda_2$  is not close to  $\tau$ . Guided by the numerical results, we pose the following scalings:

$$Rs = \Gamma^{-n} \widetilde{Rs}; \quad k^2 = \Gamma^{(1-2n)/3} \tilde{k}^2; \quad Ra^{(o)} = \Gamma^{-(2+2n)/3} \widetilde{Ra}; \quad \omega^2 \sim k^2/2\Gamma = \Gamma^{-(2+2n)/3} \tilde{\omega}^2. \quad (3.3)$$

Note that  $Ra_c^{(o)}$  determined under the scalings (3.3) will be asymptotically smaller than  $Ra_c^{(o)}$  for the classical problem (in which, from (2.28),  $Ra_c^{(o)}$  and  $Rs$  are of the same order).

When  $n > 2$  we can define the small parameter  $\varepsilon = \Gamma^{(n-2)/3}$ . We then make an expansion in powers of  $\varepsilon$ , with the expansion carried as far as  $\varepsilon^2 = \Gamma^{(2n-4)/3}$ . Since  $k^2$  is assumed large, we can replace  $\beta^2 = k^2 + 1$  by  $k^2$ , since the error in doing this is  $O(\Gamma^{(2n-1)/3}) = O(\Gamma\varepsilon^2)$ .

The leading terms in (2.23) suggest the *ansatz*

$$\omega^2 = \frac{1}{\lambda_2} \left( \frac{\tilde{k}^2}{2} + \varepsilon p_1 + \varepsilon^2 p_2 \right) \Gamma^{-(2+2n)/3}. \quad (3.4)$$

On substituting expression (3.4) into (2.23), we find, correct to  $O(\varepsilon^2)$ ,

$$b_6 \omega^6 = 2\sigma \lambda_1^2 \lambda_2^{-1} \left( \tilde{k}^8 + 6\varepsilon p_1 \tilde{k}^6 + 12\varepsilon^2 p_1^2 \tilde{k}^4 + 6\varepsilon^2 p_2 \tilde{k}^6 \right) \Gamma^{(7-8n)/3}, \quad (3.5a)$$

$$b_4 \omega^4 = \left( -2\sigma \left( \lambda_1^2 \lambda_2^{-1} + 2\tau \lambda_1 \right) \tilde{k}^8 - 8\varepsilon \sigma \left( \lambda_1^2 \lambda_2^{-1} + 2\tau \lambda_1 \right) p_1 \tilde{k}^6 + \varepsilon^2 \left( \sigma + (1 + \sigma) \lambda_1^2 \lambda_2^{-2} \right) \tilde{k}^6 \right. \\ \left. - 8\varepsilon^2 \sigma \left( \lambda_1^2 \lambda_2^{-1} + 2\tau \lambda_1 \right) \left( p_2 \tilde{k}^2 + p_1^2 \tilde{k}^4 \right) \right) \Gamma^{(7-8n)/3}, \quad (3.5b)$$

$$b_2 \omega^2 = \left( 2\sigma \tau \left( \tau \lambda_2 + 2\lambda_1 \right) \tilde{k}^8 + \varepsilon \left( 2\sigma \left( \tau \lambda_2 - \lambda_1^2 \lambda_2^{-1} \right) \widetilde{Rs} \tilde{k}^4 + 4\sigma \tau \left( \tau \lambda_2 + 2\lambda_1 \right) p_1 \tilde{k}^6 \right) \right. \\ \left. + \varepsilon^2 \left( 4\sigma \tau \left( \tau \lambda_2 + 2\lambda_1 \right) p_2 \tilde{k}^6 + 4\sigma \left( \tau \lambda_2 - \lambda_1^2 \lambda_2^{-1} \right) p_1 \widetilde{Rs} \tilde{k}^2 \right. \right. \\ \left. \left. - \left( \sigma + 2\tau \left( 1 + \sigma \right) \lambda_1 \lambda_2^{-1} \right) \tilde{k}^6 \right) \right) \Gamma^{(7-8n)/3}, \quad (3.5c)$$

$$b_0 = \left( -2\sigma \tau^2 \lambda_2 \tilde{k}^8 + 2\varepsilon \sigma \tau \left( \lambda_1 - \lambda_2 \right) \widetilde{Rs} \tilde{k}^4 + \varepsilon^2 \tau^2 \left( 1 + \sigma \right) \tilde{k}^6 \right) \Gamma^{(7-8n)/3}. \quad (3.5d)$$

369 By construction, the leading order terms in (2.23) cancel. At  $O(\varepsilon)$  we find

$$370 \quad p_1 = \frac{\lambda_1 \widetilde{R}s}{2(\lambda_1 - \tau\lambda_2)\widetilde{k}^2}, \quad (3.6)$$

371 and at  $O(\varepsilon^2)$  we obtain

$$372 \quad 16p_1^2\sigma \left( \lambda_1^2\lambda_2^{-1} - \tau\lambda_1 \right) \widetilde{k}^4 + \left( 4p_2\sigma\lambda_2^{-1} + (1+\sigma)\lambda_2^{-2} \right) (\lambda_1 - \tau\lambda_2)^2 \widetilde{k}^6 \\ 373 \quad \quad \quad + 4p_1\sigma\lambda_2^{-1} \left( \tau\lambda_2^2 - \lambda_1^2 \right) \widetilde{R}s\widetilde{k}^2 = 0. \quad (3.7)$$

375 Finally, substituting for  $p_1$  from (3.6) into (3.7) yields

$$376 \quad p_2 = -\frac{1}{4} \left( \frac{1+\sigma}{\lambda_2\sigma} + \frac{2\lambda_1(\lambda_1^2 + \tau\lambda_2^2)\widetilde{R}s^2}{(\lambda_1 - \tau\lambda_2)^3\widetilde{k}^6} \right). \quad (3.8)$$

377 We have now found the expression of  $\omega^2$  correct to order  $\varepsilon^2$  in expansion (3.4). To determine  
378 the corresponding value of the critical Rayleigh number, we substitute for  $\omega^2$  into either of  
379 the equations (2.22); expanding as before and cancelling a common factor of  $\Gamma$ , we obtain  
380 the following expressions for the various terms in, for example, (2.22b):

$$381 \quad a_4\omega^4 = \frac{\lambda_1}{\lambda_2}\widetilde{k}^8 + 4\varepsilon\frac{\lambda_1}{\lambda_2}p_1\widetilde{k}^6 + \varepsilon^2 \left( 4\frac{\lambda_1}{\lambda_2}(p_2\widetilde{k}^6 + p_1^2\widetilde{k}^4) + \frac{1}{2\lambda_2^2\sigma}\widetilde{k}^6 \right), \quad (3.9a)$$

$$382 \quad a_2\omega^2 = \frac{1}{\lambda_2} \left[ (\tau\lambda_2 + \lambda_1)\widetilde{k}^8 + \varepsilon \left( \widetilde{R}s\widetilde{k}^4 + 2(\tau\lambda_2 + \lambda_1)p_1\widetilde{k}^6 \right) \right. \\ 383 \quad \left. + \varepsilon^2 \left( 2(\tau\lambda_2 + \lambda_1)p_2\widetilde{k}^6 + 2\widetilde{R}s p_1\widetilde{k}^2 + \frac{1}{2} \left( (1 + (1 + \tau)/\sigma)\widetilde{k}^6 - 2\widetilde{R}a\widetilde{k}^4 \right) \right) \right], \quad (3.9b)$$

$$384 \quad a_0 = \tau\widetilde{k}^8 + \varepsilon\widetilde{R}s\widetilde{k}^4 - \varepsilon^2\tau\widetilde{R}a\widetilde{k}^4. \quad (3.9c)$$

386 It is easily checked that both the  $O(1)$  and  $O(\varepsilon)$  terms in (2.22b) cancel; the remaining terms  
387 lead to the relatively simple relation

$$388 \quad \widetilde{R}a = \frac{\widetilde{k}^2}{2\lambda_2} + \frac{\lambda_1^2\widetilde{R}s^2}{(\tau\lambda_2 - \lambda_1)^2\widetilde{k}^4} \implies Ra^{(o)} = \frac{\Gamma^{-1}k^2}{2\lambda_2} + \frac{\lambda_1^2Rs^2}{(\tau\lambda_2 - \lambda_1)^2k^4}. \quad (3.10)$$

389 Minimising  $Ra^{(o)}$  with respect to  $k^2$  determines the critical values  $k_c^2$  and  $Ra_c^{(o)}$  as

$$390 \quad k_c^2 = \left( \frac{4\lambda_1^2\lambda_2\Gamma Rs^2}{(\tau\lambda_2 - \lambda_1)^2} \right)^{\frac{1}{3}}, \quad Ra_c^{(o)} = \frac{3}{2\lambda_2} \left( \frac{\lambda_1^2\lambda_2\Gamma^{-2}Rs^2}{2(\tau\lambda_2 - \lambda_1)^2} \right)^{\frac{1}{3}}. \quad (3.11)$$

391 The asymptotic results (3.11) are plotted in figure 4. As expected, the agreement with the  
392 full system improves with increasing  $n$ ; for  $n = 4$  and  $n = 5$  the asymptotic and numerical  
393 results are almost indistinguishable, except in the immediate neighbourhood of the dip, where  
394 expressions (3.11) diverge. In each case, the classical stability boundary is at a much higher  
395 value of  $Ra$ , and so is not shown.

396 It is interesting to relate the above results to those for  $\lambda = \pm 1$  obtained in Paper I. From the  
397 expression for  $Ra_c^{(o)}$  in (3.11) we can calculate the position of the minimum in the  $Ra$  vs  $\lambda$   
398 curve, which is at  $\lambda = -1 + 2\sqrt{\tau/(1+\tau)}$ . We note that at this minimum,  $Ra = O(\Gamma^{-(2+2n)/3})$ ,  
399 whereas, when  $\lambda = -1$ , different asymptotic scalings apply.

400 For  $\lambda = -1$ ,

$$401 \quad Ra \approx \Gamma^{-1}(Rs/\tau)^{1/2} = O(\Gamma^{-(1+n/2)}); \quad (3.12)$$

402 hence the smallest value of  $\widetilde{Ra}_c$  always occurs at  $\lambda = -1$  ( $C_s = 0$ ). How then does the  
 403 solution approach  $\lambda = -1$ ? Assuming that the full solution varies slowly with  $\lambda$  near  $\lambda = -1$ ,  
 404 we can estimate where the internal solution given by (3.11) attains the ‘left hand’ value.  
 405 Assuming  $\lambda_1$  is small (and hence  $\lambda_2 \approx 1$ ), we find an intersection of the two solutions when  
 406  $\lambda = -1 + \delta\lambda_1$  where

$$407 \quad \delta\lambda_1 = O((Rs/\tau\Gamma^2)^{-1/4}); \quad (3.13)$$

408 this is small when  $n \gtrsim 3$ .

409 Near  $\lambda = 1$  ( $\lambda_2 = 0$ ), on the other hand, (3.11) implies  $Ra = O(\Gamma^{-2/3}(Rs/\lambda_2)^{2/3})$  as  
 410  $\lambda_2 \rightarrow 0$ . However, the scaling for  $\lambda = 1$  gives

$$411 \quad Ra \approx \sigma Rs/(1 + \sigma). \quad (3.14)$$

412 Matching these two results is accomplished through a boundary layer of thickness  $\delta\lambda_2$ , where

$$413 \quad \delta\lambda_2 = O\left((1 + \sigma^{-1})^{3/2}(\Gamma^2 Rs)^{-1/2}\right). \quad (3.15)$$

### 414 3.3.2. Asymptotics near the dip

415 Near the critical value  $\lambda_d = (\tau - 1)/(\tau + 1)$  different asymptotics apply, as can be seen from  
 416 the numerical results, which give a much lower critical wavenumber. This much smaller  
 417 wavenumber mode exists for a range of  $\lambda$ , but the analysis is easier when  $\lambda$  is close to  $\lambda_d$ .  
 418 For the time being, then, we set

$$419 \quad \lambda_1 = \lambda_2(\tau + \gamma\kappa), \quad (3.16)$$

420 where we introduce the expansion parameter  $\delta = \Gamma^{(n/2-1)} \ll 1$  ( $n > 2$ ), and write  $\gamma = \delta/\lambda_2$ .  
 421 Following numerical evidence, we write  $Ra = \Gamma^{-n}\widetilde{Ra}$ ,  $k^2 = \Gamma^{-n/2}\widetilde{k}^2$  (note that these differ  
 422 from the scalings in § 3.3.1), and carry our analysis to  $O(\delta)$ . As in § 3.3.1, since  $k^2 \gg 1$  we  
 423 would like to approximate  $\beta^2 = 1 + k^2$  by  $k^2$ . The error due to such an approximation is then  
 424 of relative order  $\Gamma^{n/2}$ , while we need to carry the expansion only to  $O(\delta) \gg \Gamma^{n/2}$ . Thus to  
 425 this order we can write  $\beta^2 = k^2$  throughout.

426 Keeping the two leading order terms in the coefficients of (2.24) gives

$$427 \quad b_6 = 16\sigma(\tau^2 + 2\gamma\tau\kappa)\lambda_2^4\widetilde{k}^2\Gamma^{4-n/2}, \quad (3.17a)$$

$$428 \quad b_4 = \left(-24\sigma\tau^2\widetilde{k}^4 - 32\gamma\sigma\tau\kappa\widetilde{k}^4 + 4\gamma(\sigma + (1 + \sigma)\tau^2)\widetilde{k}^2\right)\lambda_2^3\Gamma^{3-n}, \quad (3.17b)$$

$$429 \quad b_2 = \left(12\sigma\tau^2\widetilde{k}^6 + 4\sigma\tau(1 - \tau)\widetilde{Rs}\widetilde{k}^2 + 8\gamma\sigma\tau\kappa\widetilde{k}^6 - 8\gamma\sigma\tau\kappa\widetilde{Rs}\widetilde{k}^2\right. \\ 430 \quad \left.- 2\gamma(\sigma + 2\tau^2(1 + \sigma))\widetilde{k}^4\right)\lambda_2^2\Gamma^{2-3n/2}, \quad (3.17c)$$

$$431 \quad b_0 = \left(-2\sigma\tau^2\widetilde{k}^8 - 2\sigma\tau(1 - \tau)\widetilde{Rs}\widetilde{k}^4\right. \\ 432 \quad \left.+ \gamma\tau^2(1 + \sigma)\widetilde{k}^6 + 2\gamma\sigma\tau\kappa\widetilde{Rs}\widetilde{k}^4 - \gamma\sigma(1 - \tau)\widetilde{Rs}\widetilde{k}^2\right)\lambda_2\Gamma^{1-2n}. \quad (3.17d)$$

434 Note that in expressions (3.17), we have not expanded the  $\lambda_2$  terms into their  $O(1)$  and  $O(\gamma)$   
 435 components. It turns out that there is significant cancellation of the  $\lambda_2$  terms in equation (2.23)  
 436 and we therefore defer to a later stage any  $\lambda_2$  terms that remain.

437 It is easily verified that when  $\gamma = 0$ , equation (2.23) (with coefficients (3.17)) is solved by

$$438 \quad \omega^2 = \frac{1}{2\lambda_2}\widetilde{k}^2\Gamma^{-1-n/2} = \frac{1}{2\lambda_2}k^2\Gamma^{-n/2}. \quad (3.18)$$

439 To obtain the next order correction to  $\omega^2$ , we thus write

$$440 \quad \omega^2 = \frac{1}{2\lambda_2} \left( \tilde{k}^2 + \gamma p \right) \Gamma^{-1-n/2}, \quad (3.19)$$

441 where we still keep  $\lambda_2$  unexpanded. From (2.23), at  $O(\gamma)$ , there is considerable simplification;  
442 all of the factors of  $\Gamma$  and  $\lambda_2$  drop out, with the remaining terms determining  $p$  simply as

$$443 \quad p = \frac{1}{2\tau} + \frac{\tilde{k}^2 \kappa}{(1-\tau)}. \quad (3.20)$$

444 We now use (2.22b), correct to  $O(\gamma)$ , to determine  $\widetilde{Ra}$ , which we write as  $\widetilde{Ra} = \widetilde{Ra}_0 + \gamma \widetilde{Ra}_1$ .  
445 At this stage we do need to pay heed to the separate  $O(1)$  and  $O(\gamma)$  terms in  $\lambda_2$ ; thus, from  
446 (3.16), together with the relation  $\lambda_1 + \lambda_2 = 1$ , we have

$$447 \quad \lambda_2^{-1} = (1 + \tau) + \gamma \kappa. \quad (3.21)$$

448 From (2.19b,d,f), together with (3.19) – (3.21), retaining terms up to  $O(\gamma)$  and dividing out  
449 a common factor of  $\Gamma^{-2n}$ , we obtain

$$450 \quad a_4 \omega^4 = \tau \tilde{k}^8 + \gamma \left( \frac{1+\tau}{2\sigma} \tilde{k}^6 + \tilde{k}^6 + \kappa \tilde{k}^8 \left( \frac{1+\tau}{1-\tau} \right) \right), \quad (3.22a)$$

$$451 \quad a_2 \omega^2 = 2\tau \tilde{k}^8 + (1+\tau)(\widetilde{Rs} - \widetilde{Ra}_0) \tilde{k}^4$$

$$452 \quad + \gamma \left( \frac{1}{2} \left( 3 + \frac{1+\tau}{\sigma} \right) \tilde{k}^6 + \frac{1+\tau}{2\tau} (\widetilde{Rs} - \widetilde{Ra}_0) \tilde{k}^2 - (1+\tau) \widetilde{Ra}_1 \tilde{k}^4 \right)$$

$$453 \quad + \gamma \kappa \left( \frac{1}{1-\tau} \right) \left( (1+\tau) \tilde{k}^8 + 2(\widetilde{Rs} - \widetilde{Ra}_0) \tilde{k}^4 \right), \quad (3.22b)$$

$$454 \quad a_0 = \tau \tilde{k}^8 + (\widetilde{Rs} - \tau \widetilde{Ra}_0) \tilde{k}^4 - \gamma \tau \widetilde{Ra}_1 \tilde{k}^4. \quad (3.22c)$$

456 On substituting from expressions (3.22) into (2.22b), the  $O(1)$  and  $O(\gamma)$  terms give

$$457 \quad \widetilde{Ra}_0 = \tau \widetilde{Rs}, \quad \widetilde{Ra}_1 = \frac{1}{2} \left( \tilde{k}^2 + \frac{1}{\tau \tilde{k}^2} (1 - \tau^2) \widetilde{Rs} \right) + 2\kappa \widetilde{Rs}, \quad (3.23)$$

458 or, in unscaled variables,

$$459 \quad Ra^{(o)} = \tau Rs + \gamma \left( \frac{\Gamma^{-n/2}}{2} \left( k^2 + \frac{1}{\tau k^2} (1 - \tau^2) Rs \right) + 2\kappa Rs \right). \quad (3.24)$$

460 Thus  $Ra^{(o)}$  is minimised when

$$461 \quad k_c^4 = \frac{1}{\tau} (1 - \tau^2) Rs, \quad (3.25)$$

462 which is independent of  $\kappa$  at leading order. The excellent agreement between the asymptotic  
463 result (3.25) and the full numerical result is shown in figure 5. It should just be noted that  
464 in the dip,  $Ra_c^{(o)}$  ( $= \tau Rs$  at leading order, from (3.23)) and  $Ra_c^{(s)}$  ( $= Rs/\tau$  at leading order,  
465 from (2.21)) are of the same asymptotic order ( $O(\Gamma^{-n})$ ). However, the oscillatory mode is  
466 always preferred since  $\tau < 1$ . Furthermore,  $Ra_c^{(o)}$  in the dip ( $= \tau Rs$ ) is also of the same  
467 asymptotic order as  $Ra_c^{(o)}$  for the classical problem ( $= (\sigma + \tau)/(1 + \sigma) Rs$  at leading order,  
468 from (2.28)). Since  $\tau < 1$ , it follows that, even in the dip,  $Ra_c^{(o)}$  for the M-C problem with  
469  $n \geq 3$  is lower than that of the classical problem.

470 Expression (3.25) describes the depth of the dip. Its lateral extent in  $\lambda$  can be estimated by  
471 equating the values of  $Ra_c^{(o)}$  for the outer solution, given by (3.11), with the value of  $Ra_c^{(o)}$

472 for the inner (dip) solution, which, to leading order, is given by  $Ra = \tau Rs$ , from (3.23). If  
 473 we write  $\lambda = \lambda_d + \delta$  then, to leading order, (3.11) gives

$$474 \quad Ra_c^{(o)} = 3 \left( \frac{\tau Rs}{2\Gamma\delta(1+\tau)} \right)^{2/3}. \quad (3.26)$$

475 Equating expression (3.26) with  $\tau Rs$  leads to the following estimate of  $\delta$ , the half-width of  
 476 the dip:

$$477 \quad \delta = \frac{3^{3/2}}{2\Gamma(1+\tau)(\tau Rs)^{1/2}}. \quad (3.27)$$

478 The decrease in the width of the dip with increasing  $Rs$  can be clearly seen in figure 5.

### 479 3.3.3. Low wavenumber modes

480 The analysis of § 3.3.2 shows that the preferred mode at the dip is a high wavenumber mode,  
 481 with  $k_c^2 = O(\Gamma^{-n/2})$  and  $Ra_c^{(o)} = O(\Gamma^{-n})$ . For completeness, it is though worth noting that  
 482 there is also a minimum in the  $(k^2, Ra^{(o)})$  curve at very low wavenumbers. Guided by the  
 483 numerical results, the relevant scalings for this low wave-number mode are  $k^2 = O(\Gamma^{n-1})$ ,  $\omega^2 =$   
 484  $O(\Gamma^{-1})$ ,  $Ra^{(o)} = O(\Gamma^{-n})$ : we may thus write  $k^2 = \Gamma^{n-1}\tilde{k}^2$ ,  $\omega^2 = \Gamma^{-1}\tilde{\omega}^2$ ,  $Rs = \Gamma^{-n}\tilde{Rs}$ ,  
 485  $Ra = \Gamma^{-n}\tilde{Ra}$ . With these scalings, the dominant balance in the frequency equation (2.23) is  
 486 between the  $b_2\omega^2$  and  $b_0$  terms, giving, to leading order,

$$487 \quad \tilde{\omega}^2 = \left( \frac{\sigma(1-\tau)}{1+\sigma} \right) \tilde{Rs}\tilde{k}^2. \quad (3.28)$$

488 At leading order, (2.22b) gives

$$489 \quad \tilde{Ra}^{(o)} = \frac{\frac{2}{\sigma}\tilde{\omega}^4 - \left(1 + \frac{(1+\tau)}{\sigma} + 2\tilde{Rs}\tilde{k}^2\right)\tilde{\omega}^2 + \tilde{Rs}\tilde{k}^2}{\tilde{k}^2(\tau - 2\tilde{\omega}^2)}, \quad (3.29)$$

490 which simplifies, using (3.28), to

$$491 \quad \tilde{Ra}^{(o)} = \left( \frac{\sigma + \tau}{1 + \sigma} \right) \tilde{Rs} \implies Ra^{(o)} = \left( \frac{\sigma + \tau}{1 + \sigma} \right) Rs. \quad (3.30)$$

492 The  $k^2$  dependence has dropped out at this order, so to determine  $k_c^2$  we would need to go to  
 493 higher order. However, this is unnecessary, since the value of  $Ra^{(o)}$  for the high wavenumber  
 494 mode at the dip ( $Ra^{(o)} = \tau Rs$  from (3.23)), although of the same order asymptotically as  
 495  $Ra^{(o)}$  given by (3.30) (i.e.  $O(\Gamma^{-n})$ ), is always lower (recalling that  $\tau < 1$ ). Thus, in the first  
 496 quadrant, the low-wavenumber mode is never preferred.

### 497 3.3.4. Varying $\tau$ and $\sigma$

498 In this subsection we consider, numerically, the effects of varying  $\tau$  and  $\sigma$ . Figure 7 shows  
 499  $Ra_c^{(o)}$ ,  $k_c^2$  and  $\omega_c^2$  as functions of  $\lambda$  for  $n = 3$  with  $\sigma = 1$  and for three different values of  $\tau$   
 500 (the  $\tau = 0.5$  results are as plotted in figures 4(a-c)). It can be seen clearly that increasing  $\tau$   
 501 leads to the dip in  $k_c^2$  becoming deeper and narrower, in accordance with expressions (3.25)  
 502 and (3.27). The wider picture, taken across all  $\tau$ , is provided by the surface plots in figure 8,  
 503 which show  $Ra_c^{(o)}$  and  $k_c^2$  as functions of  $\lambda$  and  $\tau$ ; the dip is the prominent valley in the  $k_c^2$   
 504 surface.

505 In terms of varying  $\sigma$ , the general picture is unchanged between  $\sigma = O(1)$  and  $\sigma \gg 1$ ,  
 506 as illustrated by figure 9, which shows  $Ra_c^{(o)}$ ,  $k_c^2$  and  $\omega_c^2$  as functions of  $\lambda$  for  $\sigma = 1, 5,$   
 507  $10$ . There are strong variations in  $k_c^2$  and  $\omega_c^2$  (but not  $Ra_c^{(o)}$ ) near  $\lambda = -1$  to adjust to their

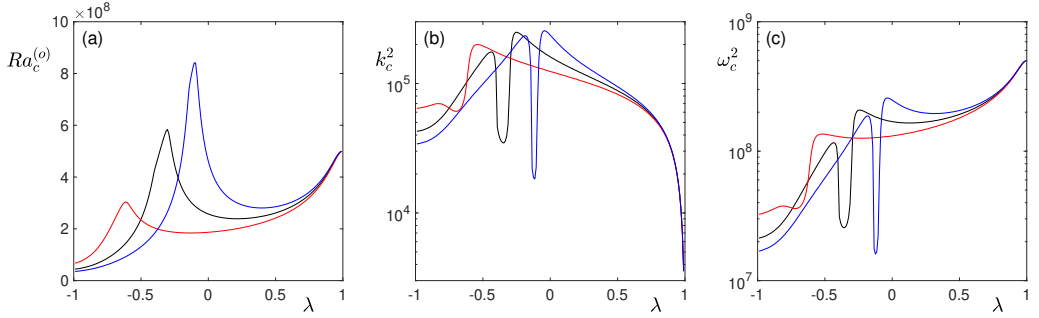


Figure 7:  $Ra_c^{(o)}$ ,  $k_c^2$  and  $\omega_c^2$  versus  $\lambda$  for  $\Gamma = 10^{-3}$ ,  $Rs = 10^9$ ,  $\sigma = 1$ , with  $\tau = 0.2$  (red),  $\tau = 0.5$  (black),  $\tau = 0.8$  (blue).

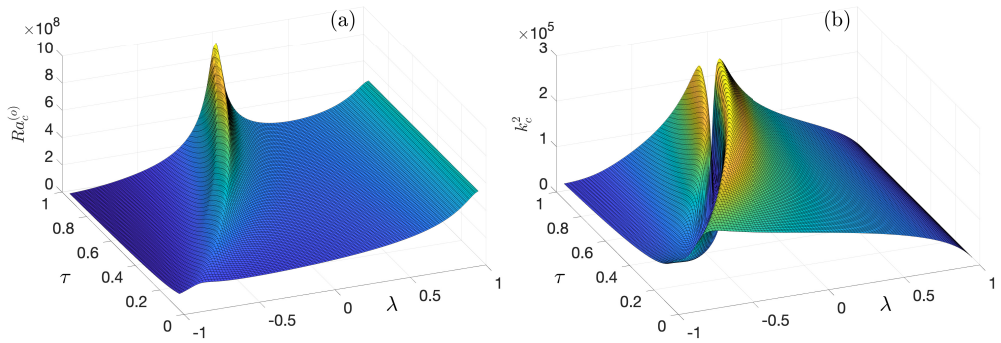


Figure 8: (a)  $Ra_c^{(o)}$  and (b)  $k_c^2$  versus  $\lambda$  and  $\tau$  for  $\Gamma = 10^{-3}$ ,  $Rs = 10^9$ ,  $\sigma = 1$ . The range  $0.05 \leq \tau \leq 0.95$  is plotted.

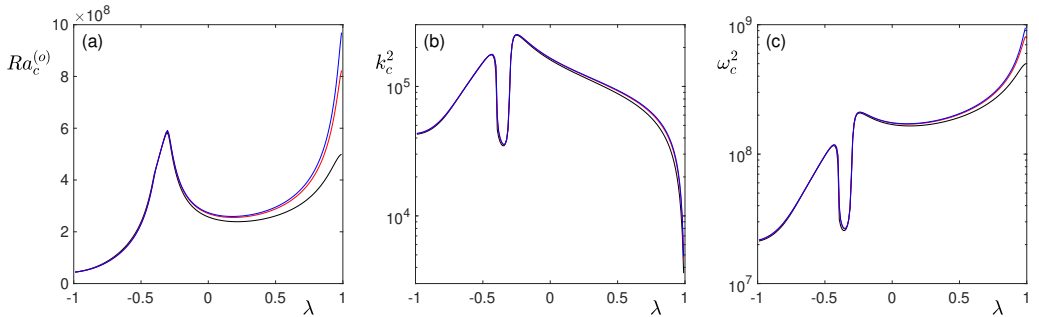


Figure 9:  $Ra_c^{(o)}$ ,  $k_c^2$  and  $\omega_c^2$  versus  $\lambda$  for  $\Gamma = 10^{-3}$ ,  $Rs = 10^9$ ,  $\tau = 0.5$ , with  $\sigma = 1$  (black),  $\sigma = 5$  (red),  $\sigma = 100$  (blue).

508 limiting values at  $\lambda = 1$  (see § 4.2.3 of Paper I). For smaller  $\sigma$ , the differences from  $\sigma = O(1)$   
 509 become more marked. Figure 10 shows  $Ra_c^{(o)}$  and  $k_c^2$  as functions of  $\lambda$  and  $\tau$  for  $\sigma = 0.075$   
 510 and  $\sigma = 0.01$ . In comparison with figure 8, it can be seen that decreasing  $\sigma$  leads to a drastic  
 511 change in the  $k_c^2$  surface for  $\lambda$  close to  $-1$ . The sides of the valley are eroded, first of all  
 512 to form just an island where higher  $k_c^2$  modes are preferred (figure 10(b)) before the valley  
 513 disappears altogether (figure 10(d)). The asymptotic analysis of § 3.3.1, performed under  
 514 the assumption that  $\sigma \gtrsim O(1)$ , and leading to the results (3.11), is clearly no longer valid.

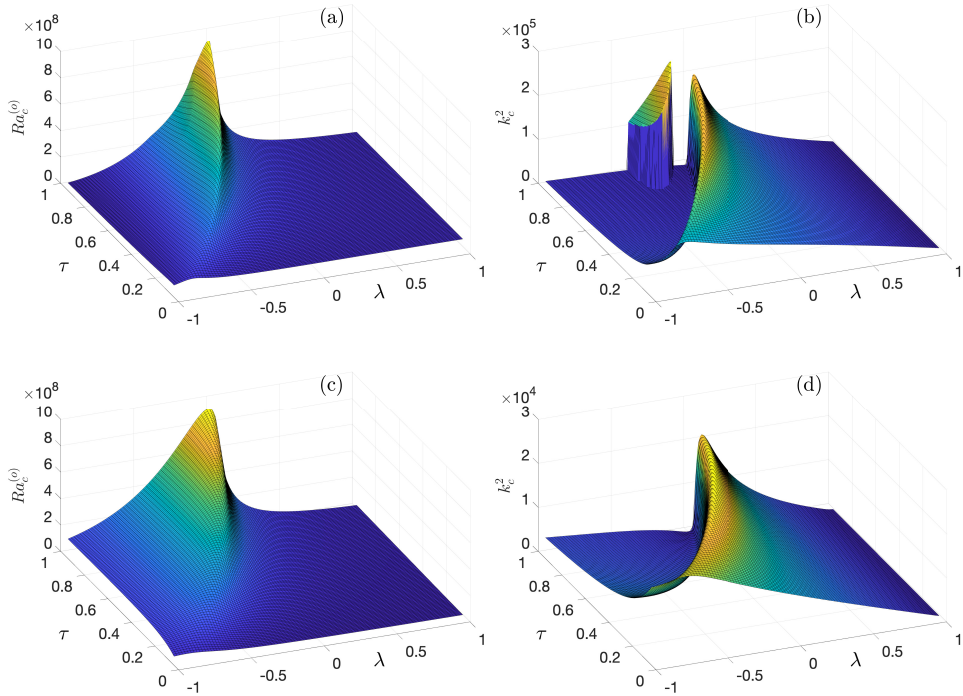


Figure 10: (a, c)  $Ra_c^{(o)}$  and (b, d)  $k_c^2$  versus  $\lambda$  and  $\tau$  for  $\Gamma = 10^{-3}$ ,  $Rs = 10^9$ . In (a, b),  $\sigma = 0.075$ ; in (c, d),  $\sigma = 0.01$ . The range  $0.05 \leq \tau \leq 0.95$  is plotted.

515 Indeed, one can see that the ordering adopted in § 3.3.1 breaks down once  $\sigma$  is as small as  
 516  $O(\Gamma^{(n-2)/3})$ ; i.e. when  $\sigma = O(10^{-1})$  for the parameter values of figure 10. Analysing small  
 517  $\sigma$  requires a separate asymptotic ordering (or orderings) along the lines pursued by Hughes  
 518 *et al.* (2022) in their analysis of the Maxwell-Cattaneo effect in rotating convection: as this  
 519 would essentially be a further paper in itself, we have restricted our detailed attention here  
 520 to the case of  $\sigma \gtrsim O(1)$ .

#### 521 4. The third quadrant: $Rs < 0$ , $Ra < 0$

522 In the classical double-diffusive problem ( $\Gamma = 0$ ), the onset of instability in the third quadrant  
 523 is always via a direct instability; the steady mode remains the favoured mode of instability  
 524 for  $n < 2$ . However, once  $\Gamma^2 Rs$  is of order unity, oscillations can be preferred at onset. These  
 525 oscillations can arise in a number of ways depending on the value of  $\lambda$ . We first consider the  
 526 transitional case of  $n = 2$ . Here there are two different scenarios, described in § 4.1 and § 4.2.  
 527 The former occurs in a range of  $\lambda$  including  $\lambda = -1$ , where the latter holds for larger values  
 528 of  $\lambda$ , in a range including  $\lambda = 1$ . We call these cases ‘smaller  $\lambda$ ’ and ‘larger  $\lambda$ ’ respectively.  
 529 The global picture for  $n = 2$ , across all  $\lambda$ , is illustrated in § 4.3. We then consider the situation  
 530 where  $n > 2$ , where oscillatory behaviour is generally well established. High wavenumber  
 531 modes are considered in § 4.4 and low wavenumber modes in § 4.5; these are combined to  
 532 give the full stability picture in § 4.6.

533 Since many of the results of the preceding section do not seem to depend on the signs of  
 534  $Ra$  and  $Rs$ , it might be thought that they could be adapted straightforwardly to the analysis  
 535 of the third quadrant. However, this is not the case. The analogues of minima of  $Ra$  in the

536 first quadrant are usually maxima of  $Ra$  in the third quadrant, so there is no relation between  
 537 the preferred wavenumbers in the two cases. In the third quadrant, oscillations appear only  
 538 if  $n$  is sufficiently large and so the way in which they manifest themselves needs detailed  
 539 investigation, while in the first quadrant oscillations are possible for all  $n > 0$ . Finally,  
 540 the third quadrant counterpart of the remarkable ‘dip’ phenomenon encountered in the first  
 541 quadrant differs markedly, as it leads to a region of steady convection rather than a significant  
 542 change in the oscillation wavenumber.

#### 543 4.1. $n = 2$ : Appearance of oscillations for smaller $\lambda$

544 We first look for the onset of oscillations in the third quadrant for  $n = 2$ , when  $\lambda$  is sufficiently  
 545 negative; in this case, the situation is similar to that described in Paper I for  $\lambda = -1$ . Provided  
 546  $\sigma$  is sufficiently small, oscillations appear as a loop of marginal solutions, either above or  
 547 below the steady branch, depending on the parameters.

548 We have performed a series of numerical calculations to establish the dependence of the  
 549 critical values of  $Ra$ ,  $k^2$  and  $\omega^2$  on  $\Gamma$ . Guided by these results, we deduce that the relevant  
 550 scalings are  $Ra, Rs = O(\Gamma^{-2})$ ,  $k^2 = O(\Gamma^{-1/2})$ ,  $\omega^2 = O(\Gamma^{-2})$ : thus we write  $Rs = \Gamma^{-2}\widetilde{Rs}$ ,  
 551  $Ra = \Gamma^{-2}\widetilde{Ra}$ ,  $k^2 = \Gamma^{-1/2}\widetilde{k}^2$ ,  $\omega^2 = \Gamma^{-2}\widetilde{\omega}^2$ . At leading order, the coefficients of (2.19) then  
 552 become

$$553 \quad a_5 = (1 - \lambda^2) \frac{\widetilde{k}^2}{\sigma} \Gamma^{3/2}, \quad (4.1a)$$

$$554 \quad a_4 = \frac{2}{\sigma} \widetilde{k}^2 \Gamma^{1/2}, \quad (4.1b)$$

$$555 \quad a_3 = \left( \frac{\widetilde{k}^2}{\sigma} + (1 - \lambda^2)(\widetilde{Rs} - \widetilde{Ra})\widetilde{k}^2 \right) \Gamma^{-1/2}, \quad (4.1c)$$

$$556 \quad a_2 = 2 \left( \widetilde{Rs} - \widetilde{Ra} \right) \widetilde{k}^2 \Gamma^{-3/2}, \quad (4.1d)$$

$$557 \quad a_1 = \left( \widetilde{Rs} - \widetilde{Ra} \right) \widetilde{k}^2 \Gamma^{-5/2}, \quad (4.1e)$$

$$558 \quad a_0 = \left( \widetilde{Rs} - \tau \widetilde{Ra} \right) \widetilde{k}^4 \Gamma^{-3}. \quad (4.1f)$$

560 The dominant balance in (2.22b) is then between the  $a_4\omega^4$  and  $a_2\omega^2$  terms, giving, at leading  
 561 order,

$$562 \quad \widetilde{\omega}^2 - \sigma \left( \widetilde{Rs} - \widetilde{Ra} \right) = 0. \quad (4.2)$$

563 Turning to the cubic equation for the frequency, equation (2.23), making the same scaling  
 564 and keeping only the leading terms, leads to the reduced set of coefficients,

$$565 \quad b_6 = \sigma \left( 1 - \lambda^2 \right)^2 \widetilde{k}^2 \Gamma^{7/2}, \quad (4.3a)$$

$$566 \quad b_4 = \left( 2\sigma(1 + \lambda^2) + (1 + \lambda^2) \right) \widetilde{k}^2 \Gamma^{3/2}, \quad (4.3b)$$

$$567 \quad b_2 = \left( (1 + \sigma)\widetilde{k}^2 + \sigma \left( (\tau - 1)\lambda^2 - 2(1 + \tau)\lambda + \tau - 1 \right) \widetilde{Rs}\widetilde{k}^2 \right) \Gamma^{-1/2}, \quad (4.3c)$$

$$568 \quad b_0 = -\sigma(1 - \tau)\widetilde{Rs}\widetilde{k}^2 \Gamma^{-5/2}. \quad (4.3d)$$

571 Thus equation (2.23) can be written at leading order as

$$\begin{aligned}
 & \sigma (1 - \lambda^2)^2 \tilde{\omega}^6 + \left( 2\sigma(1 + \lambda^2) + (1 + \lambda)^2 \right) \tilde{\omega}^4 \\
 572 & \quad + \left( (1 + \sigma) - \sigma \left( (1 - \tau)\lambda^2 + 2(1 + \tau)\lambda + 1 - \tau \right) \widetilde{R}s \right) \tilde{\omega}^2 - \sigma(1 - \tau)\widetilde{R}s = 0.
 \end{aligned} \tag{4.4}$$

573 In principle, (4.4) can be used to analyse the appearance of loops of marginal oscillations,  
 574 as in Paper I, although analytical results are in general too elaborate to be useful. We can,  
 575 however, look for the conditions for which one side of the loop crosses the steady branch, so  
 576 that  $\widetilde{R}s = \tau\widetilde{R}a$ , or, in view of (4.2),

$$577 \quad \tilde{\omega}^2 = -\frac{\sigma(1 - \tau)\widetilde{R}s}{\tau}. \tag{4.5}$$

578 On substituting for  $\widetilde{R}s$  from (4.5) into (4.4), we see that a factor of  $\tilde{\omega}^2$  may be cancelled,  
 579 leaving the quadratic for  $\tilde{\omega}^2$ ,

$$580 \quad \sigma \tilde{\omega}^4 (1 - \lambda^2)^2 + \tilde{\omega}^2 \left( (\lambda^2 + 1)(1 + 2\sigma + \tau) + 2\lambda \frac{1 + \tau^2}{1 - \tau} \right) + (1 + \sigma + \tau) = 0. \tag{4.6}$$

581 Equation (4.6) can have real positive solutions for  $\tilde{\omega}^2$  only if  $\lambda$  is not too large. In fact,  $\lambda$  must  
 582 satisfy the following inequality (' $b^2 > 4ac$ ')

$$583 \quad \lambda^2 \left( \sqrt{1 + \sigma + \tau} - \sqrt{\sigma} \right)^2 + \frac{2\lambda(1 + \tau^2)}{1 - \tau} + \left( \sqrt{1 + \sigma + \tau} + \sqrt{\sigma} \right)^2 < 0. \tag{4.7}$$

584 After a little algebra, we find that this inequality for  $\lambda$  is equivalent to

$$585 \quad \lambda < \frac{-(1 - \tau)}{(\sqrt{1 + \sigma + \tau} - \sqrt{\sigma})^2}. \tag{4.8}$$

586 (The root of larger modulus is less than  $-1$  and thus impermissible.) We have to check that  
 587 the value of  $\lambda$  given by (4.8) is greater than  $-1$ . Replacing the inequality by an equality and  
 588  $\lambda$  by  $-1$ , we find

$$589 \quad \sqrt{\sigma(1 + \sigma + \tau)} = \sigma + \tau, \quad \text{and hence } \sigma = \sigma_c = \frac{\tau^2}{1 - \tau}, \tag{4.9}$$

590 consistent with the results of Paper I. Thus if  $\sigma < \sigma_c$  there will be a range of negative  $\lambda$ ,  
 591 and an associated range of  $\tilde{\omega}^2$  and hence  $\widetilde{R}s$ , for which the onset of oscillations is coincident  
 592 with the steady branch when  $\widetilde{R}a = \widetilde{R}s/\tau$ . If  $\sigma > \sigma_c$ , on the other hand, oscillations are not  
 593 preferred until  $n \geq 3$ . The two different scenarios will be discussed further in § 4.3.

594 In Paper I, we showed that depending on the values of  $\sigma$  and  $\tau$ , the loop of oscillations  
 595 appears either above the steady branch, in which case the transition to oscillatory convection  
 596 occurs when the smaller of the two roots for  $|\widetilde{R}s|$  from (4.5) and (4.6) crosses the line of  
 597 the steady branch; or below the steady branch, in which case oscillations are preferred just  
 598 after the point of appearance. The transition between these two regimes occurs on a line  $\mathcal{L}$   
 599 in  $(\sigma, \tau)$  space for each  $\lambda$ ; for  $\lambda = -1$  this is given by expression (3.29) in Paper I.

600 For the case of general  $\lambda$ , we can make some progress in finding this line by returning to  
 601 (4.4), which can be written compactly as

$$602 \quad A\tilde{\omega}^6 + B\tilde{\omega}^4 + (C - D\widetilde{R}s)\tilde{\omega}^2 - E\widetilde{R}s = 0, \tag{4.10}$$

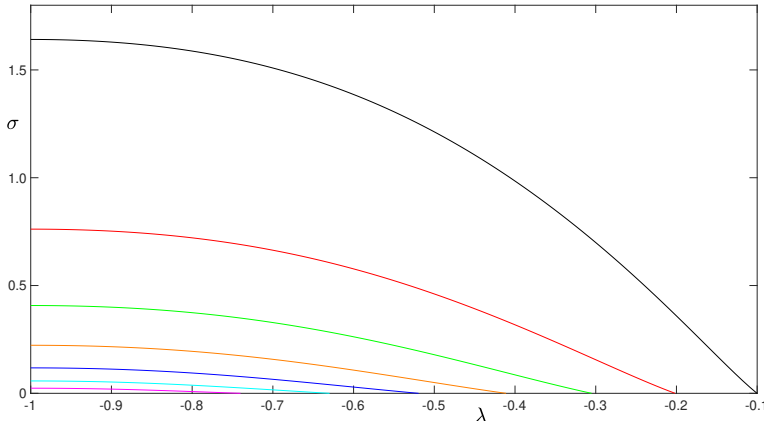


Figure 11:  $\sigma$  versus  $\lambda$  for the line  $\mathcal{L}$ , defined by (4.15), denoting the parameter values at which the loop of oscillatory solutions first appears on the steady branch. The curves show  $\tau = 0.9$  (top), 0.8, 0.7, 0.6, 0.5, 0.4, 0.3 (bottom).

604 where

$$\begin{aligned} A &= \sigma \left(1 - \lambda^2\right)^2, \quad B = 2\sigma(1 + \lambda^2) + (1 + \lambda)^2, \quad C = (1 + \sigma), \\ D &= \sigma \left((1 - \tau)(1 + \lambda^2) + 2\lambda(1 + \tau)\right), \quad E = \sigma(1 - \tau). \end{aligned} \quad (4.11)$$

606 If (4.10) has a double root, marking the appearance of the loop of oscillations, then we also  
607 have

$$3A\tilde{\omega}^4 + 2B\tilde{\omega}^2 + (C - D\tilde{R}s) = 0. \quad (4.12)$$

609 Combining (4.10) with (4.12) to eliminate the cubic term in  $\tilde{\omega}^2$  gives a further quadratic in  
610  $\tilde{\omega}^2$ ,

$$B\tilde{\omega}^4 + 2(C - D\tilde{R}s)\tilde{\omega}^2 - 3E\tilde{R}s = 0. \quad (4.13)$$

612 We now seek the condition that the loop appears on the steady branch, and hence can use  
613 expression (4.5) in (4.13). On cancelling a factor of  $\tilde{R}s$ , we obtain the following explicit  
614 formula relating the value of  $\tilde{R}s$  to the other parameters:

$$\tilde{R}s = \frac{\tau(3\tau + 2(1 + \sigma))}{\sigma((1 + \lambda^2)(1 - \tau)(1 + 2(\tau + \sigma)) + 2\lambda(1 + \tau + 2\tau^2))} = \frac{F(\sigma, \tau)}{\sigma G(\sigma, \tau, \lambda)}, \text{ say.} \quad (4.14)$$

616 Since  $\tilde{R}s < 0$ , this shows that  $\lambda$  cannot be too large, and in particular must be negative.  
617 On substituting for  $\tilde{\omega}^2$  and  $\tilde{R}s$  from (4.5) and (4.14) into (4.12), we obtain the following  
618 complicated relation defining the transition line  $\mathcal{L}$ :

$$3A\sigma(1 - \tau)^2 F^2 - 2B\sigma\tau(1 - \tau)FG + \tau^2 G(\sigma CG - DF) = 0. \quad (4.15)$$

620 The line  $\mathcal{L}$  is shown for  $\sigma$  as a function of  $\lambda$  for a number of values of  $\tau$  in figure 11. Each of  
621 the curves, which have different fixed values of  $\tau$ , denotes the value of  $\sigma$ , as a function of  $\lambda$ ,  
622 for which the loop of oscillatory solutions appears precisely on the steady branch. Above the  
623 curve (i.e. at greater values of  $\sigma$ ), the loop of oscillatory solutions is born above the steady  
624 branch; below the curve (i.e. at smaller  $\sigma$ ), the loop of oscillatory solutions is born below  
625 the steady branch.

4.2.  $n = 2$ : Appearance of oscillations for larger  $\lambda$

626

627 As has been shown above, loops of oscillations cannot appear if  $\lambda$  is too large. For larger  
628 values of  $\lambda$ , branches of oscillations can appear via Takens-Bogdanov (T-B) bifurcations  
629 from the steady branch. This situation is similar to that described in Paper I for  $\lambda = 1$ .

630

In contrast to the oscillation loops described above, the branches that appear for larger  
631  $\lambda$  have  $k^2 \sim \Gamma^{-1}$ . The T-B points are characterised by  $a_0 = a_1 = 0$  in (2.19). Writing  
632  $k^2 = \Gamma^{-1}\tilde{k}^2$ ,  $R_s = \Gamma^{-2}\tilde{R}_s$ ,  $R_a = \Gamma^{-2}\tilde{R}_a$ , and replacing  $\beta^2$  by  $k^2$  since  $k^2 \gg 1$ , we obtain

633

$$\tau\tilde{k}^4 + \tilde{R}_s - \tau\tilde{R}_a = \left(1 + \tau + \frac{\tau}{\sigma}\right)\tilde{k}^4 + \tilde{R}_s(1 + (1 + \lambda)\tilde{k}^2) - \tilde{R}_a(1 + \tau(1 - \lambda)\tilde{k}^2) = 0. \quad (4.16)$$

634

Eliminating  $\tilde{R}_a$  between the two equations of (4.16) gives the following cubic for  $\tilde{k}^2$ :

635

$$\tau(1 - \lambda)\tilde{k}^6 - \tau\left(1 + \frac{1}{\sigma}\right)\tilde{k}^4 - 2\lambda\tilde{R}_s\tilde{k}^2 + \tilde{R}_s\left(\frac{1}{\tau} - 1\right) = 0. \quad (4.17)$$

636

There are thus either one or three T-B points (noting that  $\tilde{R}_s < 0$  and that we must have  
637  $\tilde{k}^2 > 0$ ). It is instructive to consider the condition under which two T-B points coincide; this  
638 results from setting the discriminant of the cubic equation (4.17) to zero, giving

639

$$32(1 - \lambda)\lambda^3 S^2 + \left(4\lambda^2 P^2 - 36\lambda(1 - \lambda)PQ - 27(1 - \lambda)^2 Q^2\right) - 4P^3 Q = 0, \quad (4.18)$$

640

where, to simplify notation, we have introduced  $P = 1 + 1/\sigma$ ,  $Q = 1 - 1/\tau$ ,  $S = \tilde{R}_s/\tau$ .  
641 The quadratic expression (4.18) for  $S$  denotes the two values of  $S$  (and hence  $\tilde{R}_s$ ) between  
642 which there are three T-B points. By seeking the condition for these two values of  $R_s$  to be  
643 repeated, we may then identify the critical values of  $\lambda$  at which the possibility of three T-B  
644 points disappears. Setting the discriminant of the quadratic (4.18) to zero gives

645

$$\left(4\lambda^2 P^2 - 36\lambda(1 - \lambda)PQ - 27(1 - \lambda)^2 Q^2\right)^2 + 512\lambda^3(1 - \lambda)P^3 Q = 0. \quad (4.19)$$

646

On making the further substitutions

647

$$C = \lambda P, \quad D = (1 - \lambda)Q, \quad C = \Delta D, \quad \text{where} \quad \Delta = -\frac{\lambda(1 + \sigma)\tau}{(1 - \lambda)\sigma(1 - \tau)}, \quad (4.20)$$

648

we obtain a (quartic) expression involving only  $\Delta$ , which, rather remarkably, factorises as

649

$$0 = (4\Delta^2 - 36\Delta - 27)^2 + 512\Delta^3 = 16(\Delta + 9/2)^3(\Delta + 1/2). \quad (4.21)$$

650

On rearranging the expression for  $\Delta$  in (4.20), the two distinct roots of (4.21) thus give the  
651 following values of  $\lambda$  for which there are coincident T-B points:

652

$$\lambda_a = \frac{9\sigma(1 - \tau)}{9\sigma + 2\tau - 7\sigma\tau} \quad \text{and} \quad \lambda_b = \frac{\sigma(1 - \tau)}{\sigma + 2\tau + \sigma\tau}. \quad (4.22)$$

653

Recall that here we are interested in the third quadrant, and so  $R_s < 0$ ; this in turn requires  
654 (recalling  $Q < 0$ ) that the coefficient of  $S$  in equation (4.18) is positive. We find that only  
655 for  $\lambda = \lambda_a$  ( $\Delta = -9/2$ ) is this satisfied. Thus we have the possibility of three T-B points  
656 (depending on the value of  $\tilde{R}_s$ ) for  $1 > \lambda > \lambda_a$  and one T-B point otherwise. (The value  $\lambda_b$   
657 denotes such a transition point in the first quadrant. However, oscillatory modes are favoured  
658 there, with the steady mode out of contention, as discussed in § 3; T-B points thus play no  
659 role in determining the overall stability boundary in the first quadrant.)

660

The role of the T-B points can be seen through numerical calculation of the steady and  
661 oscillatory boundaries for  $\lambda < \lambda_a$  and  $\lambda > \lambda_a$ . For illustration, we consider the case of  
662  $\sigma = 0.2$ ,  $\tau = 0.5$ , for which  $\lambda_a = 3/7 \approx 0.429$ . Figure 12 shows the stability boundaries

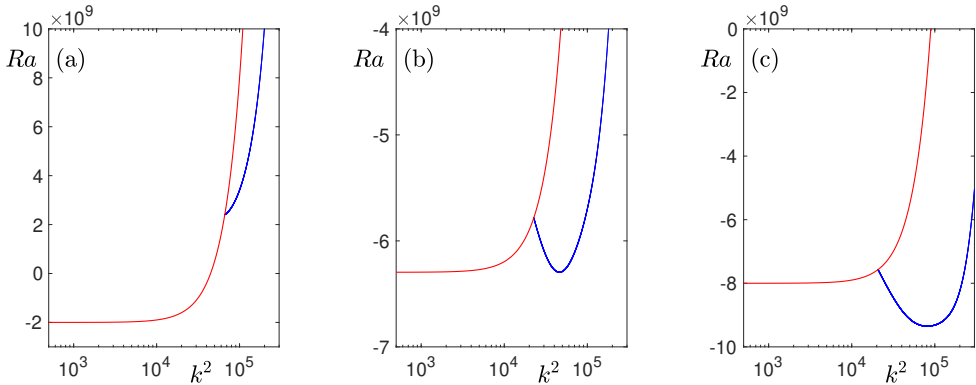


Figure 12:  $Ra$  versus  $k^2$  for the steady (red) and oscillatory (blue) stability boundaries, with  $\Gamma = 10^{-4}$ ,  $\sigma = 0.2$ ,  $\tau = 0.5$ ,  $\lambda = 0.3$ . In (a),  $R_s = -10^9$  ( $\widetilde{R}_s = -10$ ); in (b),  $R_s = -3.148 \times 10^9$  ( $\widetilde{R}_s = -31.48$ ); in (c),  $R_s = -4 \times 10^9$  ( $\widetilde{R}_s = -40$ ).

663 for  $\lambda = 0.3$ , for which there can only be one T-B point. In figure 12(a),  $\widetilde{R}_s = -10$ ; the  
 664 oscillatory branch emerging from the T-B point always lies above the minimum of the steady  
 665 branch (given by  $Ra_c^{(s)} = R_s/\tau$ ), and thus steady convection is favoured. In figure 12(b),  
 666  $\widetilde{R}_s = -31.48$ , the value at which the critical Rayleigh numbers for the (low-wavenumber)  
 667 steady and (high-wavenumber) oscillatory modes are identical. In figure 12(c),  $\widetilde{R}_s = -40$ ;  
 668 although the T-B point itself lies above  $Ra = Ra_c^{(s)}$ , the oscillatory branch emerging from  
 669 the T-B points dips down sufficiently that high-wavenumber oscillatory modes are favoured.

670 For  $\lambda > \lambda_a$ , where there is always a range of  $\widetilde{R}_s$  for which there are three T-B points,  
 671 we have identified two ways in which the oscillatory branches can evolve, dependent on the  
 672 proximity of  $\lambda$  to  $\lambda_a$ . Figures 13(a-c) show the stability boundaries for  $\lambda = 0.5$ ; i.e. for  $\lambda$   
 673 slightly greater than  $\lambda_a$ . There are three T-B points in the range  $-10.945 < \widetilde{R}_s < -9.868$ .  
 674 Figure 13(a) shows the loop of oscillatory solutions created at  $\widetilde{R}_s = -9.868$ , together  
 675 with the branch of oscillatory solutions emerging from the higher T-B point. Note that steady  
 676 solutions are preferred. At  $\widetilde{R}_s = -10.945$ , shown in figure 13(b), the two oscillatory branches  
 677 have merged, via coalescence of the upper two T-B points; again, steady solutions are still  
 678 preferred. For  $\widetilde{R}_s < -10.945$  there is only one oscillatory branch; for sufficiently negative  
 679 values of  $\widetilde{R}_s$ , oscillatory solutions become preferred, as shown in figure 13(c).

680 Figures 13(d-f) show the stability boundaries for  $\lambda = 0.8$ ; i.e. for  $\lambda$  now rather greater  
 681 than  $\lambda_a$ . There are three T-B points in the range  $-14.681 < \widetilde{R}_s < -4.490$ . We can see from  
 682 figure 13(d) that the loop of oscillatory solutions created at  $\widetilde{R}_s = -4.490$  and the branch of  
 683 oscillatory solutions emerging from the higher T-B point have both developed a pronounced  
 684 ‘hook’. Furthermore, by this value of  $\widetilde{R}_s$ , oscillatory modes have already become preferred.  
 685 As  $\widetilde{R}_s$  is made more negative, the oscillatory branches meet when  $\widetilde{R}_s = -10.466$ , as shown  
 686 in figure 13(e); in contrast to the case illustrated in figures 13(a-c), the oscillatory branches  
 687 merge before coalescence of the upper two T-B points. The oscillatory branches reconnect,  
 688 as shown in figure 13(f) for  $\widetilde{R}_s = -12$ . The upper two T-B points merge and disappear at  
 689  $\widetilde{R}_s = -14.681$ .

#### 690 4.3. Transition between steady and oscillatory onset for general $\lambda$

691 The foregoing results have shown that for sufficiently large (negative) values of  $R_s$ , oscillatory  
 692 convection can be preferred. The occurrence of oscillations in this quadrant is due entirely to

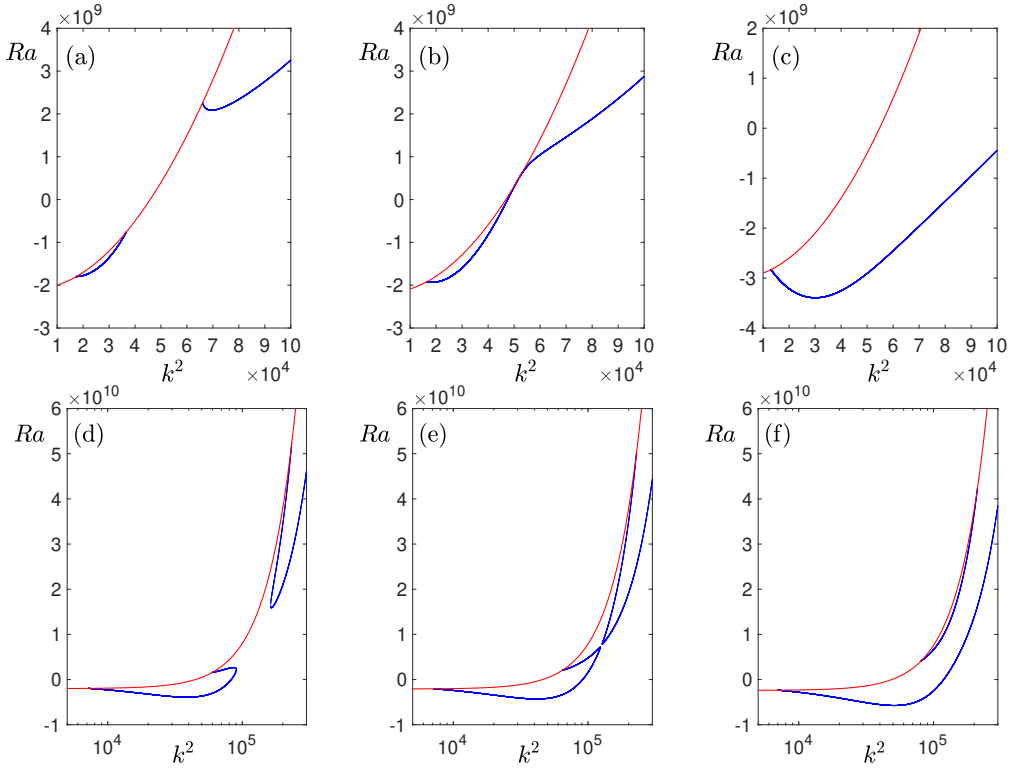


Figure 13:  $Ra$  versus  $k^2$  for the steady (red) and oscillatory (blue) stability boundaries, with  $\Gamma = 10^{-4}$ ,  $\sigma = 0.2$ ,  $\tau = 0.5$ . In (a-c),  $\lambda = 0.5$ ; in (d-f),  $\lambda = 0.8$ . In (a),  $\overline{Rs} = -10.5$  ( $Rs = -1.05 \times 10^9$ ); in (b),  $\overline{Rs} = -10.945$  ( $Rs = -1.0945 \times 10^9$ ); in (c),  $\overline{Rs} = -15$  ( $Rs = -1.5 \times 10^9$ ). In (d),  $\overline{Rs} = -10$  ( $Rs = -10^9$ ); in (e),  $\overline{Rs} = -10.466$  ( $Rs = -1.0466 \times 10^9$ ); in (f),  $\overline{Rs} = -12$  ( $Rs = -1.2 \times 10^9$ ).

693 the M-C effect, since in the classical case only steady-state bifurcations are possible. When  
 694  $\sigma < \sigma_c = \tau^2/(1 - \tau)$  (equation (4.9)), the transition to oscillatory behaviour occurs for  
 695  $|Rs| = O(\Gamma^{-n})$ , where  $\Gamma$  is generally between 2 and 3, while when  $\sigma > \sigma_c$ , oscillatory  
 696 behaviour is preferred only at values of  $n \gtrsim 3$  for smaller  $\lambda$ . The critical wavenumber of the  
 697 oscillatory mode at the transition between steady and oscillatory modes is also much larger  
 698 when  $\sigma > \sigma_c$ .

699 Figure 14 gives a global picture of the dependence of the transition values on  $\lambda$  for two  
 700 cases: (i)  $\tau = 0.5$ ,  $\sigma = 0.2$  ( $\sigma < \sigma_c$ ); (ii)  $\tau = 0.5$ ,  $\sigma = 1$  ( $\sigma > \sigma_c$ ). In this figure, the value  
 701 of  $|Rs|$  is represented by  $n$  with  $Rs = -\Gamma^{-n}$ . The curves are constructed using an iterative  
 702 process by which the critical values  $k_c^2$  and  $Ra_c^{(o)}$  are calculated for a given  $n$  and then  $n$  is  
 703 adjusted until  $Ra^{(o)} = Ra^{(s)}$  at  $n = n_c$ ,  $k_c^2 = k_{oc}^2$ . The figure thus incorporates the results of  
 704 both §4.1 and §4.2. It can be seen that in both cases the critical value  $n_c$  climbs sharply as  $\lambda$   
 705 approaches the ‘dip’ value of  $\lambda_d = (\tau - 1)/(\tau + 1)$ ;  $\lambda \approx \lambda_d$  is where anomalous behaviour of  
 706 the critical wavenumber appears in the first quadrant. As we shall show in §4.5, for  $\lambda \approx \lambda_d$   
 707 in the third quadrant, steady onset is always preferred, so that there is in fact no dip in the  
 708 critical oscillatory wavenumber in the third quadrant case.

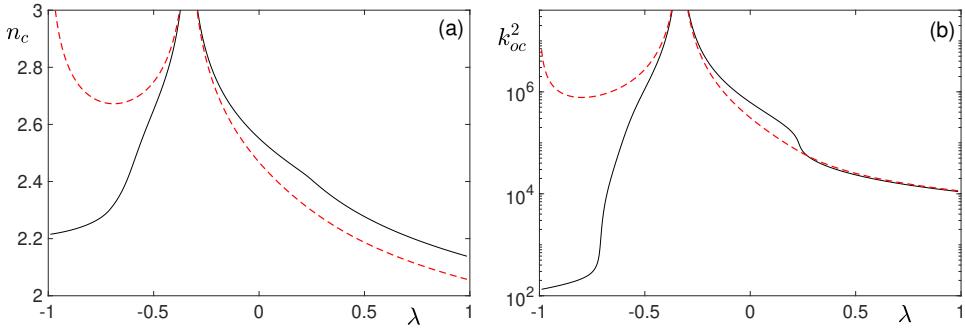


Figure 14: (a)  $n_c$  and (b)  $k_{oc}^2$  versus  $\lambda$  for  $\Gamma = 10^{-4}$ ,  $\tau = 0.5$ . The black lines denote  $\sigma = 0.2$  ( $\sigma < \sigma_c$ ), the red dashed lines  $\sigma = 1$  ( $\sigma > \sigma_c$ ).

709

#### 4.4. Instability with $n \geq 3$ : high wavenumber

710 When  $n > 2$ , and in particular when  $n \geq 3$ , oscillations are usually favoured except for  
 711 particular values of the parameters. The favoured mode of oscillation can occur either at  
 712 large or small wavenumber. In this subsection, we investigate the high wavenumber modes;  
 713 the low wavenumber modes will be discussed in § 4.5. In this high wavenumber regime,  
 714 numerical results suggest the scaling  $k^2 \sim \Gamma^{1-n}$ ; we thus write  $k^2 = \Gamma^{1-n} \tilde{k}^2$  and take  
 715  $\beta^2 = k^2$  at leading order.

716 The frequency is then determined from (2.24); with the above scaling for  $k^2$ , and assuming  
 717 that we are not particularly close to  $\lambda = \pm 1$ , so that  $1 - \lambda^2$  is not small, we find that the  
 718 coefficients of (2.24) have  $b_6 \sim \Gamma^{5-n}$ ,  $b_4 \sim \Gamma^{5-2n}$ ,  $b_2 \sim \Gamma^{5-3n}$ ,  $b_0 \sim \Gamma^{5-4n}$ . Thus, on  
 719 rescaling  $\omega^2 = \tilde{\omega}^2 \Gamma^{-n}$ , and cancelling a common factor of  $\sigma$ , we obtain the leading order  
 720 cubic equation for  $\tilde{\omega}^2$ ,

$$721 \quad (1 - \lambda^2)^2 \tilde{k}^2 \tilde{\omega}^6 - (1 - \lambda^2) (1 + 2\tau + \lambda(1 - 2\tau)) \tilde{k}^4 \tilde{\omega}^4 \\ 722 \quad + \tau \left( (\tau - 2)\lambda^2 - 2\tau\lambda + 2 + \tau \right) \tilde{k}^6 \tilde{\omega}^2 - (1 - \lambda)\tau^2 \tilde{k}^8 = 0. \quad (4.23) \\ 723$$

724 Note that the critical frequency does not depend on  $\sigma$  at leading order. On introducing  $\lambda_1, \lambda_2$   
 725 as in (2.13) and writing  $X = \tilde{\omega}^2 / \tilde{k}^2$ , (4.23) simplifies to

$$726 \quad (2\lambda_2 X - 1)(2\lambda_1 X - \tau)^2 = 0, \quad \text{so that } X = \frac{1}{2\lambda_2}, \quad X = \frac{\tau}{2\lambda_1} \quad (\text{repeated}). \quad (4.24)$$

727 We now seek to determine  $Ra$  by using the coefficients  $a_1, \dots, a_5$  defined in (2.12), and  
 728 considering (2.22b), namely  $a_4 \omega^4 - a_2 \omega^2 + a_0 = 0$ . To bring  $Ra$  into play at leading order  
 729 suggests *a priori* that  $Ra \sim k^4 \sim \Gamma^{2-2n}$ . However, for both values of  $X$  in (4.24), we find that  
 730  $Ra = 0$  in this scaling. This conclusion is supported by the numerical results. For example,  
 731 with  $n = 4$  and  $\Gamma = 10^{-4}$ ,  $Ra \sim \Gamma^{2-2n}$  would give  $Ra = O(10^{24})$ , whereas the computed  
 732 value of  $Ra_c$  is actually  $O(10^{18})$ .

733 We are thus led to the revised scalings  $k_c^2 \sim \Gamma^{1-n}$ ,  $\omega_c^2 \sim \Gamma^{-n}$ ,  $Ra_c \sim \Gamma^{1-3n/2}$ , where  
 734 the presence of  $n/2$  in the exponent of  $\Gamma$  for  $Ra_c$  derives from a half-power correction to  
 735  $X$ , which, in turn, follows from the double root in (4.24). The value of  $Ra$  corresponding  
 736 to the non-repeating root is much smaller in magnitude ( $O(\Gamma^{-n})$ ), and hence we do not  
 737 need to consider this root further. The corrections to  $b_4, b_2$  and  $b_0$  have relative magnitude  
 738  $\Gamma^{n-2}$ , which we denote by  $\varepsilon$ . Returning to using  $\tilde{\omega}^2$  and  $\tilde{k}^2$ , and now keeping the zeroth and  
 739 first-order terms, we may express (2.23) in the form

$$740 \quad b_{60} \tilde{\omega}^6 + (b_{40} + \varepsilon b_{41}) \tilde{\omega}^4 + (b_{20} + \varepsilon b_{21}) \tilde{\omega}^2 + b_{00} + \varepsilon b_{01} = 0, \quad (4.25)$$

741 where

$$742 \quad b_{60} = \sigma (1 - \lambda^2)^2, \quad (4.26a)$$

$$743 \quad b_{40} = -\sigma(1 - \lambda^2) (1 + 2\tau + \lambda(1 - 2\tau)) \tilde{k}^2, \quad (4.26b)$$

$$744 \quad b_{41} = 2\sigma(1 + \lambda^2) + (1 + \lambda)^2, \quad (4.26c)$$

$$745 \quad b_{20} = \sigma\tau \left( (\tau - 2)\lambda^2 - 2\tau\lambda + 2 + \tau \right) \tilde{k}^4, \quad (4.26d)$$

$$746 \quad b_{21} = -(\sigma + 2\tau(1 + \sigma) + \lambda(2\tau(1 + \sigma) - \sigma)) \tilde{k}^2 + \sigma \left( (\tau - 1)\lambda^2 - 2(\tau + 1)\lambda + \tau - 1 \right) \widetilde{Rs}, \quad (4.26e)$$

$$747 \quad b_{00} = -(1 - \lambda)\sigma\tau^2\tilde{k}^6, \quad (4.26f)$$

$$748 \quad b_{01} = \tau^2(1 + \sigma)\tilde{k}^4 + 2\sigma\tau\lambda\widetilde{Rs}\tilde{k}^2. \quad (4.26g)$$

750 The correction to the repeated root is  $O(\varepsilon^{1/2})$ ; thus we write

$$751 \quad \tilde{\omega}^2 = \frac{\tau\tilde{k}^2}{(1 + \lambda)} + \varepsilon^{1/2}\tilde{\omega}_1^2 = \tilde{\omega}_0^2 + \varepsilon^{1/2}\tilde{\omega}_1^2. \quad (4.27)$$

752 The  $O(\varepsilon)$  terms in (4.25) give

$$753 \quad \sigma(1 - \lambda) \left( (1 + \lambda)\tilde{\omega}_1^2 \right)^2 \left( (1 - \lambda)\tilde{\omega}_0^2 - \tilde{k}^2 \right) = -b_{41}\tilde{\omega}_0^4 - b_{21}\tilde{\omega}_0^2 - b_{01}, \quad (4.28)$$

754 which, after some algebra, leads to

$$755 \quad \tilde{\omega}_1^4 = -\frac{\tau}{(1 + \lambda)^3} \left( \tilde{k}^2 + (1 + \lambda)\widetilde{Rs} \right) = \frac{\tau}{(1 + \lambda)^3} \left( (1 + \lambda)|\widetilde{Rs}| - \tilde{k}^2 \right), \quad (4.29)$$

756 since  $Rs < 0$ . This expression is, remarkably, also independent of  $\sigma$ .

757 Using (2.22b), we can now determine the critical value of  $Ra$ . We know that at leading  
758 order,  $Ra$  does not appear. Then we may write, symbolically,

$$759 \quad \tilde{a}_4 = \tilde{a}_{40} + O(\varepsilon), \quad \tilde{a}_2 = \tilde{a}_{20} + \varepsilon^{1/2}\tilde{a}_{21} + O(\varepsilon), \quad \tilde{a}_0 = \tilde{a}_{00} + \varepsilon^{1/2}\tilde{a}_{01} + O(\varepsilon), \quad (4.30)$$

760 where the  $\tilde{a}_{21}$  and  $\tilde{a}_{01}$  terms are those containing  $Ra$ . After some algebra, the  $O(\varepsilon^{1/2})$  terms  
761 in (2.22b) give

$$762 \quad \tilde{k}^4 \left( (1 - \lambda)\tilde{\omega}_0^2 - \tilde{k}^2 \right) (1 + \lambda)\tilde{\omega}_1^2 = 2\widetilde{Ra}\tilde{k}^2\tilde{\omega}_0^2 - \tau\widetilde{Ra}\tilde{k}^4. \quad (4.31)$$

763 On substituting for  $\tilde{\omega}_0^2$  and  $\tilde{\omega}_1^2$  from (4.27) and (4.29), and rearranging, (4.31) gives

$$764 \quad \widetilde{Ra} = \widetilde{Ra}^{(o)} = -\frac{|(1 - \lambda)\tau - (1 + \lambda)|}{(1 - \lambda)(\tau(1 + \lambda))^{1/2}} \left( (1 + \lambda)|\widetilde{Rs}|\tilde{k}^4 - \tilde{k}^6 \right)^{1/2}. \quad (4.32)$$

765 We note from (4.29) that there are positive and negative roots for  $\tilde{\omega}_1^2$ ; in (4.32) we have  
766 chosen the appropriate solution for  $\tilde{\omega}_1^2$ , dependent on whether  $\lambda < \lambda_d$  or  $\lambda > \lambda_d$ , to make  
767  $\widetilde{Ra}^{(o)} < 0$ , as required. From (4.32),  $\widetilde{Ra}^{(o)}$  is minimised when

$$768 \quad \tilde{k}^2 = \tilde{k}_c^2 = \frac{2(1 + \lambda)|\widetilde{Rs}|}{3} \implies k_c^2 = \frac{2\Gamma(1 + \lambda)|Rs|}{3}, \quad (4.33)$$

769 giving

$$770 \quad \widetilde{Ra}_c^{(o)} = -\frac{2}{3^{3/2}} \left( \frac{1 + \lambda}{1 - \lambda} \right) \left( \frac{|(1 - \lambda)\tau - (1 + \lambda)|}{\tau^{1/2}} \right) |\widetilde{Rs}|^{3/2}, \quad (4.34)$$

771 or, equivalently,

$$772 \quad Ra_c^{(o)} = -\frac{2\Gamma}{3^{3/2}} \left( \frac{1+\lambda}{1-\lambda} \right) \left( \frac{|(1-\lambda)\tau - (1+\lambda)|}{\tau^{1/2}} \right) |Rs|^{3/2}. \quad (4.35)$$

773 In the scaling of this subsection,  $Ra_c^{(o)}$  vanishes (and so has a maximum) when  $\lambda = \lambda_d$ , the  
774 critical dip value in the first quadrant. In § 4.5, we discuss whether a similar dip appears in  
775 the third quadrant.

776 We note also that expression (4.35) does not hold for  $\lambda = \pm 1$  and so different scalings  
777 must apply near these endpoints. The connection between the results of this subsection and  
778 the endpoint results from Paper I are discussed below in § 4.6.

#### 779 4.5. Instability with $n \geq 3$ : low wavenumber

780 In both the first and third quadrants, there is a minimum in  $Ra^{(o)}$  at very small  $k^2$ . In general,  
781 this minimum is at a different asymptotic level to  $Ra_c^{(o)}$  at high  $k^2$  and is not of interest.  
782 However, at the dip, it can be of the same order, and so we need to establish whether low-  
783 wavenumber oscillations can be preferred (for the first quadrant low-wavenumber modes, we  
784 showed in § 3.3.3 that this was never the case).

785 Guided by numerical results, we adopt the following scalings for  $k^2$ ,  $\omega^2$  and  $Rs$ :

$$786 \quad k^2 = \Gamma^{n-2} \tilde{k}^2, \quad \omega^2 = \Gamma^{-2} \tilde{\omega}^2, \quad Rs = \Gamma^{-n} \widetilde{Rs}. \quad (4.36)$$

787 From the frequency equation (2.23),  $\tilde{\omega}^2$  obeys the following leading order equation:

$$788 \quad \sigma \left( 1 - \lambda^2 \right)^2 \tilde{\omega}^6 + \left( 2\sigma(1 + \lambda^2) + (1 + \lambda)^2 \right) \tilde{\omega}^4 + \\ 789 \quad \left( (1 + \sigma) + \sigma \left( (\tau - 1)\lambda^2 - 2(\tau + 1)\lambda + \tau - 1 \right) \widetilde{Rs} \tilde{k}^2 \right) \tilde{\omega}^2 - \sigma(1 - \tau) \widetilde{Rs} \tilde{k}^2 = 0. \\ 790 \quad (4.37)$$

791 In (2.22b), the dominant balance is between the first two terms, giving

$$792 \quad \widetilde{Ra} = \widetilde{Rs} - \frac{\tilde{\omega}^2}{\sigma \tilde{k}^2}. \quad (4.38)$$

793 Expression (4.37) determines  $\tilde{\omega}^2$  (and hence  $\widetilde{Ra}^{(o)}$  from (4.38)) as a function of  $\tilde{k}^2$ . For the  
794 critical value  $Ra_c^{(o)}$ , where  $d\widetilde{Ra}/d\tilde{k}^2 = 0$ , (4.38) implies that

$$795 \quad \frac{d\tilde{\omega}^2}{d\tilde{k}^2} = \frac{\tilde{\omega}^2}{\tilde{k}^2}. \quad (4.39)$$

796 Expressions (4.37) – (4.39) may be combined to eliminate  $\tilde{\omega}^2$ , yielding a quadratic equation  
797 for  $k_c^2$ , with one admissible root. However this does not lead to a simple formula for the  
798 critical value of  $Ra$ . That being said, we can nonetheless make progress in addressing the  
799 key point of whether the oscillatory branch can ever reach the steady branch in the dip region  
800 (which would then suggest that oscillations can be preferred for some parameter values).  
801 Substituting the critical value for the onset of steady convection ( $\widetilde{Ra} = \widetilde{Rs}/\tau$ ) into (4.38)  
802 gives

$$803 \quad \widetilde{Rs} = \frac{\tau}{\sigma(\tau - 1)} \frac{\tilde{\omega}^2}{\tilde{k}^2}. \quad (4.40)$$

804 On substituting for  $\widetilde{Rs}$  from (4.40) and for the dip value of  $\lambda = (\tau - 1)/(\tau + 1)$  into (4.37),

805 and simplifying, we then obtain the following quadratic for  $\tilde{\omega}^2$ :

$$806 \quad 16\tau^2\tilde{\omega}^4 + 4\sigma(1+\tau^2)(1+\tau)^2\tilde{\omega}^2 + (1+\sigma+\tau)(1+\tau)^4 = 0. \quad (4.41)$$

807 In principle, expression (4.41) gives the frequency of the oscillatory mode at the point where  
 808 the oscillatory branch crosses the steady branch (at the dip parameter values). However, we can  
 809 see that there are no real positive solutions for  $\tilde{\omega}^2$ . Hence the oscillatory branch never reaches  
 810 the steady branch, and so steady modes are always preferred to low wavenumber oscillations  
 811 in the dip region. Furthermore, numerical solutions and the results of § 4.4 demonstrate that  
 812 at the dip values, high wavenumber oscillations can occur only at much smaller (negative)  
 813 values of  $Ra$  than for steady convection. Thus, at the dip, the high wavenumber (oscillatory)  
 814 mode gives way to the steady branch.

#### 815 4.6. *Instability with $n \geq 3$ : combined results across all wavenumbers*

816 We have seen from the results above that when  $n \geq 3$ , the preferred mode of convection is  
 817 oscillatory over a wide range of values of  $\lambda$ . Away from the dip value  $\lambda_d$  and the endpoints  
 818  $\lambda = \pm 1$ , the dominant mode has high critical wavenumber; as  $\lambda$  approaches  $\lambda_d$ , the critical  
 819 value of  $Ra$  for oscillations increases, and for fixed  $\lambda$  near the dip is  $O(\Gamma^{1-3n/2})$ . As  $|\lambda - \lambda_d|$   
 820 becomes small,  $O(\Gamma^{n/2-1})$ , the (negative) value of  $Ra$  increases towards zero, and the  
 821 preferred mode of instability is steady convection, with critical wavenumber of order unity  
 822 and  $|Ra| = O(\Gamma^{-n})$ . There is also, in principle, an oscillatory convection mode at low  
 823 wavenumber, which near the dip can exhibit a critical value comparable with that of classical  
 824 steady convection, but this mode is never preferred.

825 The results for general  $\lambda$  away from  $\lambda_d$  cease to hold when  $\lambda$  is close to 1 or  $-1$ . Indeed,  
 826 from the results of Paper I, when  $\lambda = \pm 1$ ,  $Ra_c$  (and also  $k_c^2$  and  $\omega_c^2$ ) exhibits a different  
 827 asymptotic ordering to that displayed in (4.35). At  $\lambda = -1$ , the onset of instability is steady  
 828 if  $\sigma > \sigma_c = \tau^2/(1-\tau)$ , with

$$829 \quad Ra_c^{(s)} \approx \frac{Rs}{\tau}, \quad (4.42)$$

830 and oscillatory if  $\sigma < \sigma_c$ , with

$$831 \quad Ra_c^{(o)} \approx \frac{(\sigma + \tau)Rs}{\sigma}. \quad (4.43)$$

832 At  $\lambda = 1$ , the onset of instability is always oscillatory, with

$$833 \quad Ra_c^{(o)} \approx -\Gamma^2 Rs^2. \quad (4.44)$$

834 The transition between the result (4.35), valid for general  $\lambda$  apart from  $\lambda = \pm 1$  and at the  
 835 dip, and the end-point results (4.42)–(4.44) is achieved through boundary layers close to  
 836  $\lambda = \pm 1$ . As in § 3.3.1, we may estimate the width of the boundary layers by supposing that  
 837 the end-point solutions vary slowly with  $\lambda$ , and then finding the value of  $\lambda$  for which the  
 838 interior value of  $Ra_c$ , given by (4.35), matches the appropriate end-point value. Thus the  
 839 boundary layer close to  $\lambda = -1$  ( $\lambda_1 = 0$ ) has width

$$840 \quad \delta\lambda_1 = O\left((\Gamma^2|Rs|\tau^3)^{-1/2}\right) \quad (\sigma > \sigma_c); \quad \delta\lambda_1 = O\left((\sigma + \tau)(\sigma^2\Gamma^2|Rs|\tau)^{-1/2}\right) \quad (\sigma < \sigma_c). \quad (4.45)$$

841 Finally, the boundary layer close to  $\lambda = 1$  has width

$$842 \quad \delta\lambda_2 = O\left((\Gamma^2|Rs|\tau)^{-1/2}\right). \quad (4.46)$$

843 Figure 15 gives an overview of the behaviour of the critical values of  $Ra$ ,  $k^2$  and  $\omega^2$ ,

844 calculated numerically, as functions of  $\lambda$  in the third quadrant. The respective asymptotic  
 845 results (4.35), (4.33) and (4.27) (combined with (4.29)) are also shown. The dip, in which  
 846 the critical wavenumber is dramatically reduced and the preferred mode becomes steady for  
 847 a range of  $\lambda$ , can be clearly seen. In figures 15(a-c),  $n = 3$  and  $\sigma = 1 > \sigma_c = 0.5$ ; close to  
 848  $\lambda = -1$ , the onset of instability is thus steady. In figures 15(d-f),  $n = 3$  and  $\sigma = 0.2 < \sigma_c$ ;  
 849 the onset of instability therefore remains oscillatory up to  $\lambda = -1$ . Figures 15(g-i) are as for  
 850 figures 15(a-c), but with  $n = 4$ . In comparison with the  $n = 3$  plots, two features are apparent:  
 851 the width of the dip is markedly reduced, and the agreement between the numerical and  
 852 asymptotic results is dramatically improved.

853 Figure 16 shows the behaviour of the critical values of  $Ra$ ,  $k^2$  and  $\omega^2$  for  $n = 4$  close to  
 854  $\lambda = -1$  and  $\lambda = 1$ , highlighting the thin transition regions between the solutions at the end  
 855 point and in the interior. In figures 16(a-c),  $\sigma > \sigma_c$  and there is a transition to steady onset  
 856 in a region of width  $\delta\lambda_1$  given by (4.45) (this thin transition region is too narrow to be seen  
 857 in figures 15(g-i)). In figures 16(d-f),  $\sigma < \sigma_c$ ; onset remains oscillatory up to  $\lambda = -1$ , but  
 858 there is again a transition between the interior and end point solutions, now in a region of  
 859 width  $\delta\lambda_1$  again given by (4.45). Figures 16(g-i) show the transition between interior and  
 860 end point solutions over a region of width  $\delta\lambda_2$  given by (4.46).

861 The surface plots of figure 17 show  $Ra_c$  and  $k_c^2$  as functions of  $\lambda$  and  $\tau$  for  $\sigma = 1$  and  
 862  $n = 3$ . The  $k_c^2$  surface shows clearly the two disconnected regions of oscillatory solutions  
 863 at high values of  $k^2$ , separated by a flat valley of steady solutions, with  $k_c^2 = 0.5$ . For  
 864 small  $\tau$ , the  $Ra_c$  surface extending from  $\lambda = -1$  is flat (independent of  $\lambda$ ) before turning  
 865 downhill as the oscillatory solution is preferred. For larger values of  $\tau$ , there is a ‘bowl’ where  
 866 high-wavenumber oscillatory solutions are preferred; at such values of  $\tau$ , with increasing  $\lambda$   
 867 the surface again becomes flat after the bowl, with the steady mode preferred, before again  
 868 turning downhill as the oscillatory solution is favoured.

## 869 5. Beyond the stability boundary

870 The foregoing analysis has been directed solely at identifying the lines of neutral stability  
 871 where the preferred mode has zero growth rate. Beyond these lines the basic state is unstable,  
 872 with at least one mode having positive real part. We designate the mode that has the largest  
 873 real part of the growth rate as the ‘gravest mode’. Note that the wavenumber corresponding  
 874 to the gravest mode will normally be different from that corresponding to the (preferred)  
 875 mode with the lowest value of  $Ra$ .

876 We have shown that M-C effects destabilise, to oscillatory modes, swathes of parameter  
 877 space that are stable for the classical problem. Nonetheless, an important question is whether,  
 878 in the unstable regime, the growth rate of oscillations is relatively feeble, or whether we can  
 879 expect robustly growing oscillations well away from the stability boundary even for very  
 880 small values of  $\Gamma$  when  $Rs$  is large enough.

881 We have provided some answers to these questions by numerically calculating growth  
 882 rates, oscillation frequencies and wavenumbers for the gravest mode, over the full range of  $\lambda$   
 883 for small values of  $\Gamma$  and large values of  $|Rs|$ , where  $|Rs| = O(\Gamma^{-n})$  with  $n = 3$  and  $\Gamma = 10^{-3}$   
 884 and  $10^{-4}$ , and for the particular values  $\sigma = 1$  and  $\tau = 0.5$ . Figure 18 shows the results  
 885 for the first quadrant ( $Rs > 0$ ); for the top row,  $\Gamma = 10^{-3}$  (cf. figure 4a-c); for the bottom  
 886 row,  $\Gamma = 10^{-4}$ . In this quadrant the classical instability (when  $\Gamma = 0$ ) is oscillatory; the  
 887 classical boundary is marked, and it can be seen that MC-effects greatly increase the range  
 888 of instability. By contrast, figure 19 shows the results for the third quadrant ( $Rs < 0$ ). In this  
 889 case the classical problem has no oscillatory instabilities; the latter now become preferred  
 890 over most of the parameter space owing to the MC-effect. For the top row,  $\Gamma = 10^{-3}$  (cf.  
 891 figure 15a-c); for the bottom row  $\Gamma = 10^{-4}$ . In both these figures, attention is restricted to

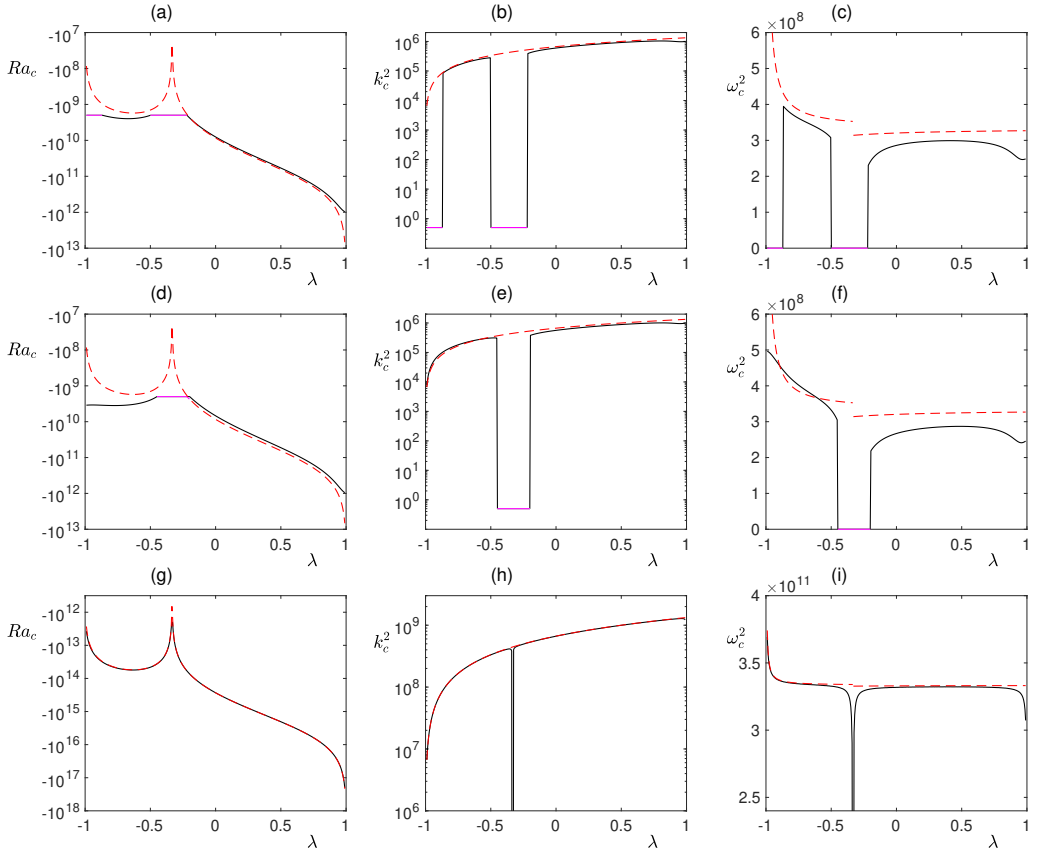


Figure 15:  $Ra_c$ ,  $k_c^2$  and  $\omega_c^2$  versus  $\lambda$ ;  $\tau = 0.5$ . In (a-c),  $\sigma = 1$ ,  $\Gamma = 10^{-3}$ ,  $Rs = -10^9$  ( $n = 3$ ); in (d-f),  $\sigma = 0.2$ ,  $\Gamma = 10^{-3}$ ,  $Rs = -10^9$  ( $n = 3$ ); in (g-i),  $\sigma = 1$ ,  $\Gamma = 10^{-3}$ ,  $Rs = -10^{12}$  ( $n = 4$ ). Numerical results are shown as solid lines; black (magenta) denotes oscillatory (steady) solutions. The asymptotic results of § 4.4 are shown as dashed red lines.

892 cases where  $Ra < Rs$ , since otherwise the system would be top heavy and hence outside of  
 893 the regime of interest for double-diffusive convection. It can be seen from both these figures  
 894 that as already discussed there are large ranges of  $Ra$  where the basic state is unstable in  
 895 the presence of M-C effects where there would be no instability in the classical case (where  
 896  $Ra > Rs/\tau$  is required for direct instability and  $Ra > Rs(\sigma + \tau)/(1 + \sigma)$  for oscillatory  
 897 instability.) Away from the stability boundary the growth rates are significant and comparable  
 898 with the oscillation frequencies. For some values of  $\lambda$  (near  $-1$  in the first quadrant, almost  
 899 everywhere in the third quadrant) oscillatory modes give way to steady modes as  $Ra$  is  
 900 increased. We note, from a comparison of the top and bottom rows of figures 18 and 19, that  
 901 reducing  $\Gamma$  with  $Rs = O(\Gamma^{-n})$  increases the region of instability; the distinguished limit of  
 902  $\Gamma \rightarrow 0$  with  $Rs = O(\Gamma^{-n})$  is in marked contrast to the straightforward limit of  $\Gamma \rightarrow 0$   
 903 with all other parameters fixed, which simply recovers the classical problem.

## 904 6. Conclusion and discussion

905 In this paper we have generalised the results presented in Paper I, in which we examined the  
 906 consequences for the onset of oscillatory double-diffusive convection when the Maxwell-

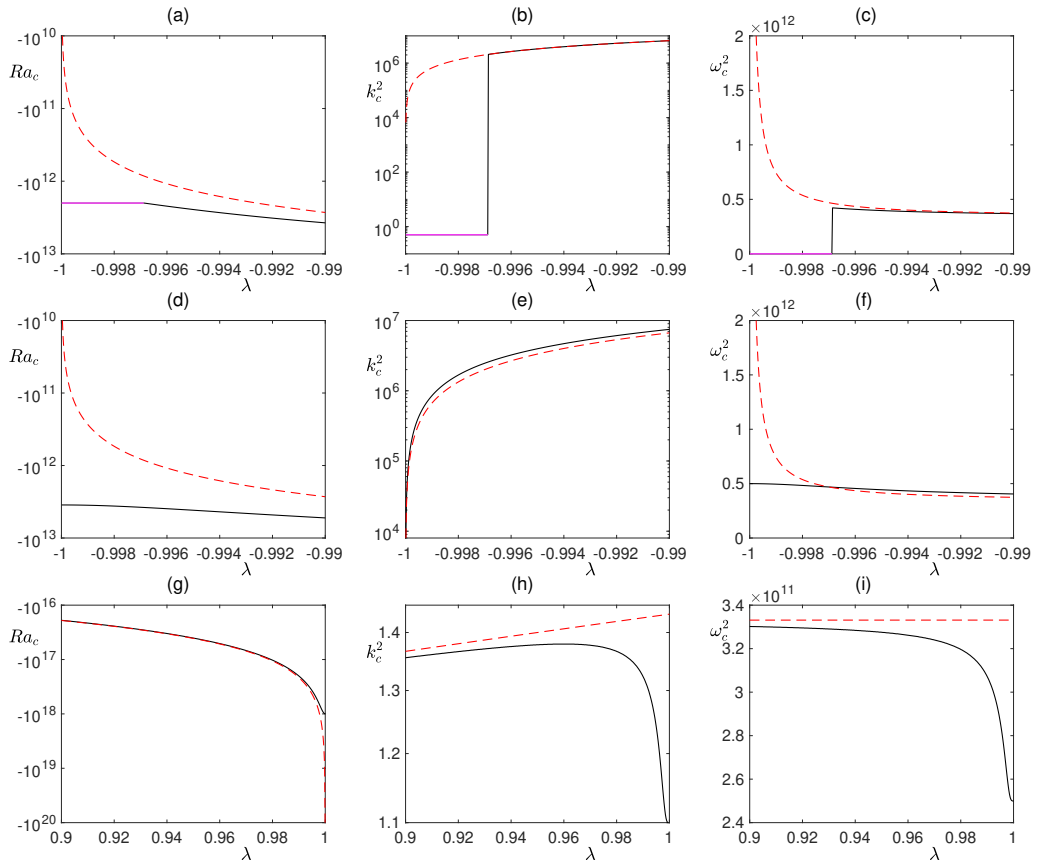


Figure 16:  $Ra_c$ ,  $k_c^2$  and  $\omega_c^2$  versus  $\lambda$ ;  $\tau = 0.5$ ,  $\Gamma = 10^{-3}$ ,  $Rs = -10^{12}$  ( $n = 4$ ). (a-c) Region near  $\lambda = -1$  for  $\sigma = 1$ ; (d-f) region near  $\lambda = -1$  for  $\sigma = 0.2$ ; (g-i) region near  $\lambda = 1$  for  $\sigma = 1$ . Numerical results are shown as solid lines; black (magenta) denotes oscillatory (steady) solutions. The asymptotic results of § 4.4 are shown as dashed red lines.

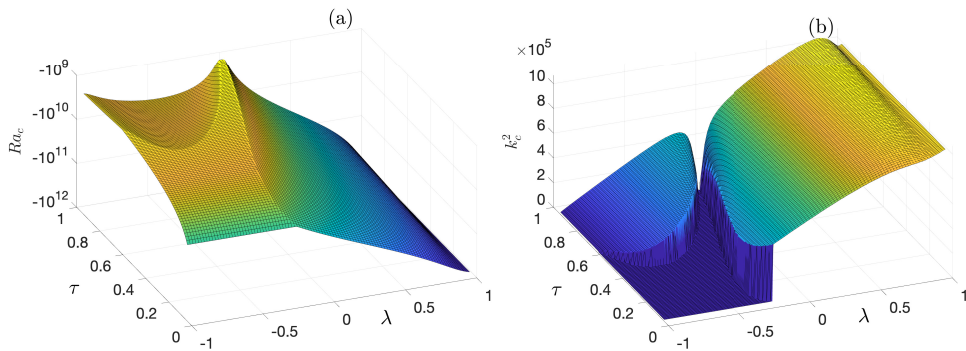


Figure 17: (a)  $Ra_c$  and (b)  $k_c^2$  versus  $\lambda$  and  $\tau$  for  $\Gamma = 10^{-3}$ ,  $Rs = -10^9$ ,  $\sigma = 1$ . The range  $0.05 \leq \tau \leq 0.95$  is plotted.

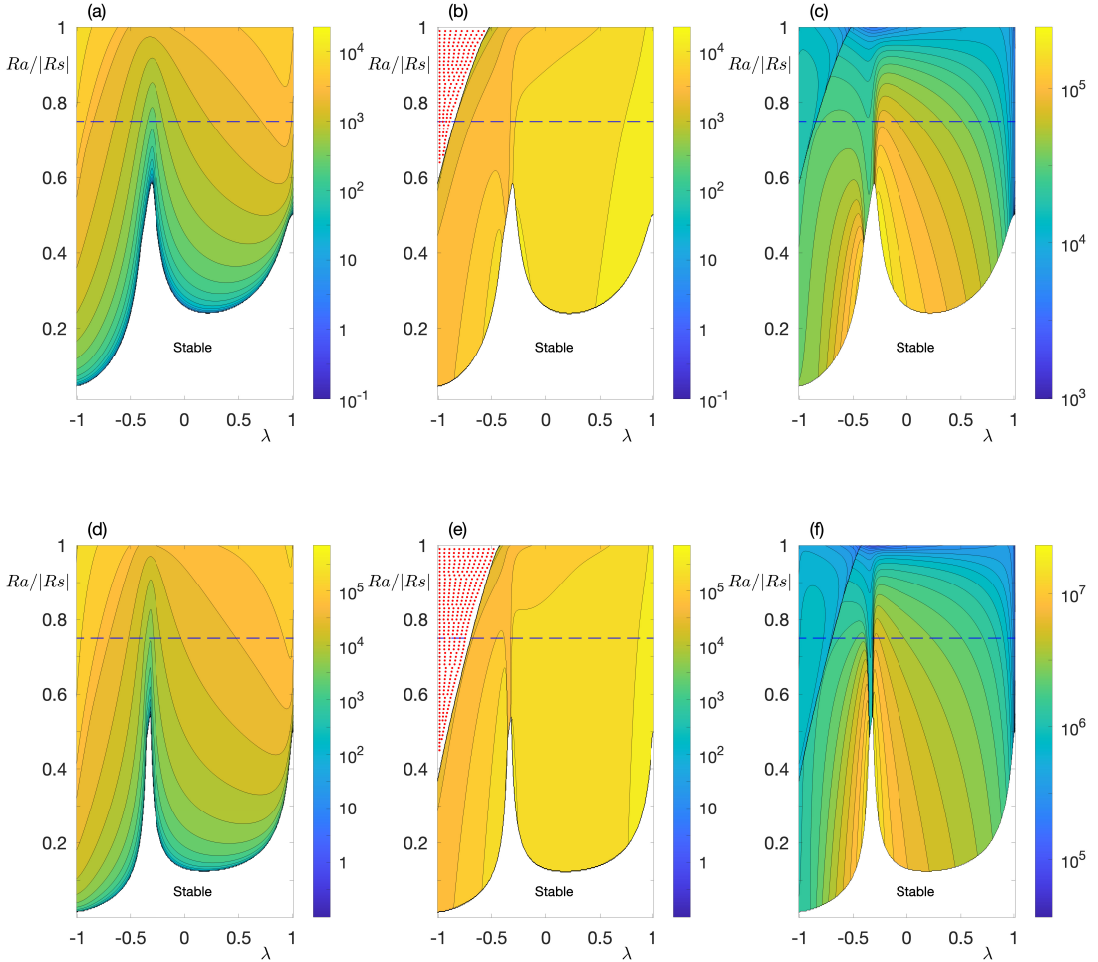


Figure 18: Contour plots as functions of  $\lambda$  and  $Ra/|Rs|$  for (a,d) growth rate, (b,e) frequency and (c,f)  $k^2$  for the gravest mode in the first quadrant;  $\sigma = 1$ ,  $\tau = 0.5$ , for the case of  $n = 3$ . In the top row,  $\Gamma = 10^{-3}$ ,  $R_s = 10^9$ ; in the bottom row,  $\Gamma = 10^{-4}$ ,  $R_s = 10^{12}$ . In plots (b) and (e), the red dotted region denotes where the gravest mode is steady. The blue dashed line shows the oscillatory stability boundary for the classical problem, given by (2.28).

907 Cattaneo (M-C) effect was in operation either for the temperature or the salinity equation,  
 908 but not both together. The important conclusion of that paper was that for sufficiently large  
 909 values of the salt gradient, the M-C effect has an important destabilising influence on the  
 910 onset of convection, and in particular it allows oscillations in the third quadrant where they  
 911 do not appear in the classical case. This is brought about through the M-C effect introducing  
 912 a new oscillatory frequency to the system, which can lead to phase relationships that are  
 913 favourable for oscillatory instability (overstability). The scaling laws for the results in the

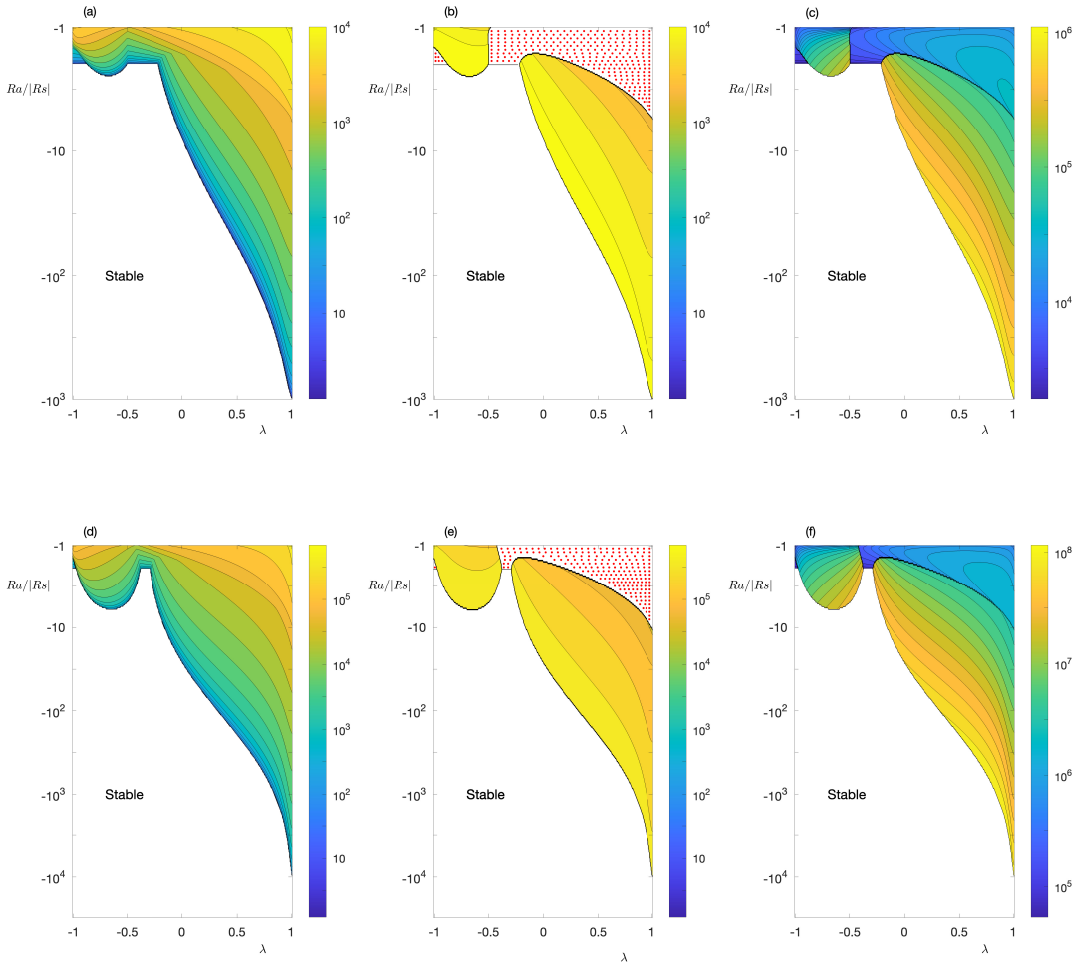


Figure 19: Contour plots as functions of  $\lambda$  and  $Ra/|Rs|$  for (a,d) growth rate, (b,e) frequency and (c,f)  $k^2$  for the gravest mode;  $\sigma = 1$ ,  $\tau = 0.5$ , for the case of  $n = 3$  in the third quadrant. In the top row,  $\Gamma = 10^{-3}$ ,  $Rs = -10^9$ ; in the bottom row,  $\Gamma = 10^{-4}$ ,  $Rs = -10^{12}$ . In plots (b) and (e), the red dotted region denotes where the gravest is steady.

914 two different cases, however, are rather different and this motivates the present study, where  
 915 the M-C effect operates on both the salt and temperature fields.

916 In contrast to the cases investigated in Paper I, we must now consider not only the  
 917 magnitudes of  $C_T$  and  $C_S$  but also their ratio; we thus introduce the quantities  $\Gamma = C_T + C_S$   
 918 and  $\lambda = (C_S - C_T)/(C_S + C_T)$ . While we can be confident that  $\Gamma$  is very small, we can be less  
 919 sure about the value of  $\lambda$ . It seems plausible on physical grounds that  $\tau_S > \tau_T$ ; however, since  
 920  $\kappa_S < \kappa$ , it is hard to pin down the ratio  $C_S/C_T \sim \kappa_S \tau_S / \kappa \tau_T$ . One should therefore investigate  
 921 the full range  $-1 < \lambda < 1$ .

922 As shown in Paper I, inclusion of the M-C effect for either temperature or salinity leads to  
 923 a surprising degree of complexity compared with the classical problem, owing to the highly

924 non-trivial dependence of the critical Rayleigh number on the wavenumber. When the M-C  
 925 effect operates on both temperature and salinity, the equation determining the square of the  
 926 oscillation frequency at onset, and also that determining the critical value of the Rayleigh  
 927 number, becomes a cubic rather than a quadratic as in the end-point cases of Paper I, thereby  
 928 adding a further layer of complexity to the problem. Nonetheless, we have been able to carry  
 929 through the analysis and determine the scalings with  $\Gamma$  for the values of the Rayleigh number  
 930 and the critical wavenumber at onset, in many cases obtaining analytical formulae valid when  
 931  $n$ , defined by  $Rs = O(\Gamma^{-n})$ , is of order 2 or greater. The accuracy of these formulae has been  
 932 confirmed by comparison with numerical calculations of the full system. The analysis has to  
 933 be carried through separately for the first and third quadrants, as the scalings generally differ.  
 934 It is assumed that (appropriately for applications) the value of  $\Gamma$ , representing the magnitude  
 935 of the new terms, is very small. For  $O(1)$  values of  $Rs$  and  $Ra$ , M-C effects are negligible.  
 936 Writing  $Rs = O(\Gamma^{-n})$ , we find that the onset of oscillatory convection in the first quadrant  
 937 is first affected by M-C effects when  $n = 1$ . While the critical wavenumber remains of order  
 938 unity, multiple extrema of the marginal stability curve can appear. In the first quadrant (§ 3),  
 939 oscillatory convection is always preferred, while multiple extrema exist for sufficiently small  
 940  $\lambda$ . In the third quadrant (§ 4), oscillations are not possible in this range of  $Rs$ , and M-C effects  
 941 become significant only when  $n = 2$ .

942 For  $n = 2$ , the M-C effect appears at the same order as other effects, and the results depend  
 943 on essentially all the terms in the governing equations (though for high wavenumber modes  
 944 we can write  $\beta^2 \approx k^2$ ). It is difficult to make much analytical progress in this regime, and  
 945 so we rely on numerical results. In the first quadrant there can be two distinct minima of  $Ra$   
 946 as a function of  $k^2$  — one at low wavenumber and the other at high wavenumber. The two  
 947 critical values of  $Ra$  are of the same order in this regime but the high wavenumber mode  
 948 always wins.

949 In the third quadrant, on the other hand, oscillations can appear as  $|Ra|$  is increased. The  
 950 way in which they appear depends on  $\sigma$  and  $\lambda$ . For sufficiently small  $\lambda$ , oscillations appear as  
 951 loops in parameter space for sufficiently small  $\sigma$ . These loops may appear above or below the  
 952 steady branch; in the former case, oscillations become preferred as  $|Rs|$  continues to increase,  
 953 while in the latter case, oscillations are preferred immediately they appear. For larger values  
 954 of  $\sigma$  no oscillations can appear until  $n \approx 3$ . For larger values of  $\lambda$ , on the other hand,  
 955 branches of oscillations will appear emanating from the steady branch via Takens-Bogdanov  
 956 bifurcations, and can subsequently become preferred.

957 For larger values of  $n$ , with  $n \gtrsim 3$ , the M-C effect generally leads to oscillatory behaviour  
 958 in both quadrants, irrespective of the values of the parameters. The new phenomenon of the  
 959 dip leads to completely different behaviour in the first quadrant close to the special value  
 960  $\lambda = \lambda_d$ , where  $C_S = \tau C_T$ , with markedly reduced critical wavenumber. (In the third quadrant,  
 961 steady convection becomes preferred near the dip location.) To try to understand these results  
 962 — and indeed in general the underlying physical consequences of the M-C effect — we can  
 963 return to the primitive equations (2.5)–(2.10). It would be ideal if the origin of the oscillatory  
 964 instability could be explicated in terms of the balances between these equations, but the  
 965 results for different parameter ranges show that the primary balances are not unique, and  
 966 that, indeed, the determination of the stability boundary is not made at leading order but  
 967 by comparing small higher order corrections. As an example, consider the situation in the  
 968 first quadrant away from the dip, for  $n \geq 3$ . Because  $Ra \ll Rs$  in this regime — see the  
 969 ordering (3.3) — the perturbed temperature  $T$  is much larger than the perturbed salinity  
 970  $S$ , and the leading order equations lead simply to free oscillations in the temperature with  
 971 frequency  $\omega$  and wavenumber  $k$  satisfying

$$972 \quad 2\Gamma\lambda_2\omega^2 = k^2. \quad (6.1)$$

973 For general values of  $\lambda$ , we can find  $S$  as an oscillation at the same frequency driven by  $T$ ,  
 974 whose relative magnitude depends on  $Ra$  and  $Rs$ . To go further, however, and determine the  
 975 size of  $Ra$  in terms of the other parameters, requires analysing the equations at higher order  
 976 and a simple physical explanation seems problematic. (This approach does, however, show  
 977 how the different scalings at the dip arise, since when  $\lambda = \lambda_d$ , there is a greatly enhanced  
 978 response from  $S$  to the oscillations in  $T$ .) Similar considerations will apply in other parameter  
 979 regimes.

980 One surprise of the present work is that the behaviour of the solutions for general  $\lambda$ , while  
 981 not dissimilar in many ways to the results of Paper I for  $\lambda = \pm 1$ , do have different asymptotic  
 982 behaviours as functions of  $\Gamma$ . A more detailed analysis would be required to understand the  
 983 transition between the asymptotic regimes as  $\lambda$  approaches 1 and  $-1$ , but this is not presented  
 984 here; only order of magnitude estimates for the transition regions are given.

985 In both the first and third quadrants, when the preferred mode is oscillatory it has a small  
 986 horizontal scale ( $k \gg 1$ ) at large  $|Rs|$ , allowing us to approximate the total wavenumber  
 987 by the horizontal wavenumber, i.e.,  $\beta^2 \approx k^2$ . Thus, to this degree of approximation, there  
 988 is a degeneracy in the vertical wavenumber  $m$ . In the numerical computations shown, we  
 989 have taken  $m = 1$ ; we have, however, also investigated the case of  $m > 1$  and found that in  
 990 all of the examples considered, the  $m = 1$  mode is preferred. We could have simplified the  
 991 equations somewhat by solving the problem in a vertically unbounded layer, although this  
 992 does have the drawback that the preferred modes for the classical instability (both steady  
 993 and oscillatory) have  $k = 0$ . Furthermore, since all the interesting instabilities induced by  
 994 the M-C effect occur at large horizontal wavenumber, our main results are unchanged. The  
 995 analysis of §§ 3,4 has revealed that new instabilities, owing their existence to the M-C effect,  
 996 can occur in parameter ranges where the classical problem has no unstable modes. It is  
 997 therefore of interest to explore the properties of these modes beyond the stability boundary.  
 998 In § 5 we therefore complement our investigations of marginal stability by calculating the  
 999 gravest modes in the unstable regime, for parameter values motivated by examples studied in  
 1000 §§ 3,4. In both the first and third quadrants, these new MC-driven modes have growth rates  
 1001 that are significant.

1002 As in Paper I, we find that, in general, oscillations are preferred in both the first and  
 1003 third quadrants when  $|Rs|$  is sufficiently large and the Prandtl number is sufficiently small.  
 1004 However, we have not investigated here the situations where  $\sigma$  scales with  $\Gamma$  to some power.  
 1005 In that case, new terms involving  $\sigma$  become important in the analysis and affect the asymptotic  
 1006 expressions. An example of the differences that can arise can be found in our parallel study  
 1007 of the effect of the M-C terms on rapidly rotating convection (Hughes *et al.* 2022). It turned  
 1008 out in that case that several different asymptotic regions exist as  $\sigma$  decreases, but the analysis  
 1009 was tractable as  $\sigma$  was the only relevant parameter. To do the same for the present problem  
 1010 would require a second extensive paper and so is left for future work.

1011 **Acknowledgements.** D.W.H. and M.R.E.P. would like to thank the Isaac Newton Institute for Mathematical  
 1012 Sciences, Cambridge, for support and hospitality during the programme *Anti-diffusive dynamics: from*  
 1013 *sub-cellular to astrophysical scales*, where work on this paper was undertaken. D.W.H. would also like to  
 1014 thank King's College, Cambridge for the award of a Visiting Fellowship.  
 1015

1016 This paper is a memorial to D.W.H. and M.R.E.P.'s coauthor Ibrahim Eltayeb, who introduced them to the  
 1017 Maxwell-Cattaneo effect and inspired the present work and a number of earlier papers, but sadly passed  
 1018 away during its preparation for publication.

1019 **Funding.** The programme at the Isaac Newton Institute was supported by EPSRC grant EP/R014604/1.

1020 **Declaration of interests.** The authors report no conflict of interest.

1021 **Author ORCIDs.** D.W. Hughes <https://orcid.org/0000-0002-8004-8631>; M.R.E. Proctor <https://orcid.org/0000-0002-2249-342X>; I.A. Eltayeb <https://orcid.org/0000-0001-7909-1483>.  
 1022

1023 **Appendix A.**

1024 Although the coefficients of the full cubic equation determining the value of  $Ra$  on the  
 1025 stability boundary for oscillatory modes are rather complicated (see supplementary material),  
 1026 and much more unwieldy than those for the cubic equation determining  $\omega^2$ , it is nonetheless  
 1027 helpful, for the  $n = 1$  regime, to work with the cubic for  $Ra$ , but just retaining the crucial  
 1028 terms. As in paper I, we scale  $R_s = \Gamma^{-1} \widetilde{R}s$ . Retaining leading order terms in the coefficients,  
 1029 and, where necessary, terms of the next order, we may express an approximation to the cubic  
 1030 equation for  $Ra$ , symbolically, by

$$1031 \quad c_{35}\Gamma^5 Ra^3 + c_{23}\Gamma^3 Ra^2 + \left(c_{11}\Gamma + c_{12}\Gamma^2\right) Ra + c_{00} + c_{01}\Gamma = 0, \quad (\text{A } 1)$$

1032 where the coefficients  $c_{ij}$  do not involve  $\Gamma$ . At leading order, we see that the smallest, and  
 1033 hence most important, root has  $Ra = O(\Gamma^{-1})$ ; thus, again as in I, we rescale  $Ra = \Gamma^{-1} \widetilde{Ra}$   
 1034 and write  $\widetilde{Ra} = \widetilde{Ra}_0 + \Gamma \widetilde{Ra}_1$ . Thus,  $\widetilde{Ra}_0 = -c_{00}/c_{11}$ , where

$$1035 \quad c_{11} = \frac{2\beta^{10}k^2(\sigma + 1)}{\sigma^4}, \quad c_{00} = -\frac{2\widetilde{R}s\beta^{10}k^2(\sigma + \tau)}{\sigma^4}, \quad (\text{A } 2)$$

1036 leading to the simple expression

$$1037 \quad \widetilde{Ra}_0 = \frac{(\sigma + \tau)}{(1 + \sigma)} \widetilde{R}s. \quad (\text{A } 3)$$

1038 Expression (A 3) is precisely as in Paper I (which looked at the cases of  $\lambda = \pm 1$ ); there is no  
 1039 wavenumber dependence and also no dependence on  $\lambda$ . The wavenumber dependence enters  
 1040 at the next order in (A 1), namely

$$1041 \quad c_{23}\widetilde{Ra}_0^2 + c_{11}\widetilde{Ra}_1 + c_{12}\widetilde{Ra}_0 + c_{01} = 0. \quad (\text{A } 4)$$

1042 On substituting for  $\widetilde{Ra}_0$  from (A 3) and for the coefficients  $c_{ij}$ , and after considerable algebra,  
 1043 we obtain the following expression for  $\widetilde{Ra}_1$ :

$$1044 \quad \widetilde{Ra}_1 = C_1 \frac{k^2}{\beta^2} + C_2 \beta^2 + C_3 \frac{\beta^6}{k^2}, \quad (\text{A } 5a)$$

1045 where

$$1046 \quad C_1 = \frac{\sigma(1 - \tau) \left[ (1 - \lambda)^2(\sigma + \tau) - (1 + \lambda)^2\tau(1 + \sigma) \right]}{(1 + \sigma)^3} \widetilde{R}s^2, \quad (\text{A } 5b)$$

$$1047 \quad C_2 = -\frac{[(1 - \lambda)(2 + \sigma)(\sigma + \tau) - (1 + \lambda)\tau(\sigma + 2\tau)(1 + \sigma)]}{(1 + \sigma)^2} \widetilde{R}s, \quad (\text{A } 5c)$$

$$1048 \quad C_3 = \frac{(\sigma + \tau)(1 + \tau)}{\sigma}. \quad (\text{A } 5d)$$

1050 Note that for  $\lambda = -1$  ( $C_s = 0$ ), expression (A 5a) reduces to expression (3.9) of Paper I; for  
 1051  $\lambda = 1$  ( $C_T = 0$ ), (A 5a) reduces to (4.8) of Paper I.

1052 Stationary points ( $d\widetilde{Ra}_1/dk^2 = 0$ ) are therefore given by the following polynomial, quintic  
 1053 in  $k^2$ :

$$1054 \quad 2C_3k^{10} + (C_2 + 7C_3)k^8 + (2C_2 + 8C_3)k^6 + (C_1 + C_2 + 2C_3)k^4 - 2C_3k^2 - C_3 = 0. \quad (\text{A } 6)$$

1055 The classical result  $k^2 = 1/2$  is recovered by setting  $C_1 = C_2 = 0$ , corresponding to  $\Gamma \rightarrow 0$   
 1056 at fixed  $R_s$ .

## REFERENCES

- 1057 CARRASSI, M. & MORRO, A. 1972 A modified Navier-Stokes equation, and its consequences on sound  
1058 dispersion. *Nuovo Cimento B Serie* **9**, 321–343.
- 1059 CHRISTOV, C. I. 2009 On frame indifferent formulation of the Maxwell-Cattaneo model of finite-speed heat  
1060 conduction. *Mech. Res. Commun.* **36**, 481–486.
- 1061 GARAUD, P. 2018 Double-diffusive convection at low Prandtl number. *Ann. Rev. Fluid Mech.* **50**, 275–298.
- 1062 HUGHES, D. W. & BRUMMELL, N. H. 2021 Double-diffusive magnetic layering. *Astrophys. J.* **922**, 195.
- 1063 HUGHES, D. W. & PROCTOR, M. R. E. 1988 Magnetic fields in the solar convection zone: magnetoconvection  
1064 and magnetic buoyancy. *Ann. Rev. Fluid Mech.* **20**, 187–223.
- 1065 HUGHES, D. W., PROCTOR, M. R. E. & ELTAYEB, I. A. 2021 Maxwell-Cattaneo double-diffusive convection:  
1066 limiting cases. *J. Fluid Mech.* **927**, A13.
- 1067 HUGHES, D. W., PROCTOR, M. R. E. & ELTAYEB, I. A. 2022 Rapidly rotating Maxwell-Cattaneo convection.  
1068 *Phys. Rev. Fluids* **7**, 093502.
- 1069 HUPPERT, H. E. & SPARKS, R.S.J. 1984 Double-diffusive convection due to crystallization in magmas. *Ann.*  
1070 *Rev. Earth Plan. Sci.* **12**, 11–37.
- 1071 HUPPERT, H. E. & TURNER, J. S. 1981 Double-diffusive convection. *J. Fluid Mech.* **106**, 299–329.
- 1072 KATO, S. 1966 Overstable convection in a medium stratified in mean molecular weight. *Publ. Astron. Soc.*  
1073 *Jpn.* **18**, 374.
- 1074 MAXWELL, J. C. 1867 On the dynamical theory of gases. *Phil. Trans. R. Soc. Lond.* **157**, 49–88.
- 1075 MERRYFIELD, W. J. 1995 Hydrodynamics of semiconvection. *Astrophys. J.* **444**, 318.
- 1076 MOHAMMADEIN, S. A. 2006 The derivation of thermal relaxation time between two-phase bubbly flow. *Heat*  
1077 *Mass Transf.* **42**, 364–369.
- 1078 NEUHAUSER, B. 1987 Thermal Relaxation in Super fluid Helium-3. *Jpn. J. Appl. Phys. Suppl.* **26** (S3-1),  
1079 187.
- 1080 RADKO, T. 2013 *Double-Diffusive Convection*. Cambridge University Press.